

Geochemistry, Geophysics, Geosystems®

RESEARCH ARTICLE

10.1029/2022GC010469

Key Points:

- Ana Slide is completely covered by 3D reflection seismic data and its kinematic development is addressed
- Large parts of the volume previously interpreted as landslide material was deformed *in-situ*
- Ana Slide developed during two separate phases that involved likely significantly smaller volumes of material than previously proposed

Supporting Information:

Supporting Information may be found in the online version of this article.

Correspondence to:

T. F. Sager,
tsager@geomar.de

Citation:

Sager, T. F., Urlaub, M., Kaminski, P., Papenberg, C., Lastras, G., Canals, M., & Berndt, C. (2022). Development and emplacement of Ana Slide, Eivissa Channel, Western Mediterranean Sea. *Geochemistry, Geophysics, Geosystems*, 23, e2022GC010469. <https://doi.org/10.1029/2022GC010469>

Received 19 MAY 2022

Accepted 5 NOV 2022

Author Contributions:

Conceptualization: Thore F. Sager, Morelia Urlaub, Christian Berndt

Data curation: Cord Papenberg, Galderic Lastras, Miquel Canals, Christian Berndt

Formal analysis: Thore F. Sager, Galderic Lastras, Miquel Canals, Christian Berndt

Funding acquisition: Morelia Urlaub, Christian Berndt

Investigation: Thore F. Sager

Methodology: Thore F. Sager, Christian Berndt

Project Administration: Morelia Urlaub, Christian Berndt

Resources: Thore F. Sager

Software: Cord Papenberg

Supervision: Thore F. Sager, Christian Berndt

Validation: Thore F. Sager, Christian Berndt

Visualization: Thore F. Sager, Christian Berndt

Writing—original draft: Thore F. Sager, Christian Berndt

Writing—review and editing: Thore F. Sager, Christian Berndt

Final approval: Thore F. Sager, Christian Berndt

Project administration: Thore F. Sager, Christian Berndt

Resources: Thore F. Sager, Christian Berndt

Software: Cord Papenberg

Supervision: Thore F. Sager, Christian Berndt

Validation: Thore F. Sager, Christian Berndt

Visualization: Thore F. Sager, Christian Berndt

Writing—original draft: Thore F. Sager, Christian Berndt

Writing—review and editing: Thore F. Sager, Christian Berndt






Final approval: Thore F. Sager, Christian Berndt

Project administration: Thore F. Sager, Christian Berndt

Resources: Thore F. Sager, Christian Berndt

Software: Cord Papenberg

Development and Emplacement of Ana Slide, Eivissa Channel, Western Mediterranean Sea

Thore F. Sager¹ , Morelia Urlaub¹, Pauline Kaminski², Cord Papenberg¹ , Galderic Lastras³ , Miquel Canals³ , and Christian Berndt¹ 

¹GEOMAR Helmholtz Centre for Ocean Research Kiel, Kiel, Germany, ²Institute of Geotechnical Engineering & Construction Management, Hamburg University of Technology (TUHH), Hamburg, Germany, ³Department of Earth and Ocean Dynamics, CRG Marine Geoscience, University of Barcelona, Barcelona, Spain

Abstract Submarine landslides can destroy seafloor infrastructures and generate devastating tsunamis. In spite of decades of research into the functioning of submarine landslides there are still numerous open questions, in particular how different phases of sliding influence each other. Here, we re-analyze Ana Slide—a relatively small (<1 km³) landslide offshore the Balearic Islands, which is unique in the published literature because it is completely imaged by high-resolution 3D reflection seismic data. Ana Slide comprises three domains: (a) a source area that is almost completely evacuated with evidence of headscarp retrogression, (b) an adjacent downslope translational domain representing a by-pass zone for the material that was mobilized in the source area, and (c) the deposit formed by the mobilized material, which accumulated downslope in a sink area and deformed slope sediment. Isochron maps show deep chaotic seismic units underneath the thickest deposits. We infer that the rapid deposition of the landslide material deformed the underlying sediments. A thin stratified sediment unit between three lobes suggests that Ana Slide evolved in two failure stages separated by several tens of thousands of years. This illustrates the problem of over-estimating the volume of mobilized material and under-estimating the complexity even of relatively simple slope failures without high-quality 3D reflection seismic data.

Plain Language Summary We investigate a submarine landslide in the Balearic Islands off Spain. The aim is to find out how such landslides work. This study is special because it can draw on a unique data set: the complete imaging of this landslide with high quality reflection seismic data. We find that previous studies have over-estimated the volume of the mobilized material because deformed sediments below the landslide were also counted, and that the slide actually consisted of two individual slope failures that occurred at the same place but in distinct episodes separated by some tens of thousands of years. Together these results show that there is a large risk of overestimating landslide-related tsunami hazards when this kind of reflection seismic data is not available.

1. Introduction

Submarine slope failures are widespread phenomena on continental margins and around ocean islands. They are often several orders of magnitude larger than their terrestrial counterparts (Varnes, 1978) and can generate devastating tsunamis that are able to inundate surrounding coastal areas while threatening infrastructure (Bondevik et al., 2005; Farrell, 1984; Haugen et al., 2005; Løvholt et al., 2017; Prior et al., 1984; Varnes, 1978). As an example a tsunami with runup heights of 8 m in western Denmark has been interpreted to have been generated by the Storegga Slide offshore Norway (Fruegaard et al., 2015).

Large-scale mass-transport deposits (MTDs) resulting from submarine slope failures have been described in many areas for example, offshore Norway (e.g., Bryn et al., 2005; Bugge et al., 1987; Haflidason et al., 2004; Kvalstad et al., 2005), in the Eastern Mediterranean Sea (Frey-Martinez et al., 2005, 2006), in the Gulf of Mexico (Sawyer et al., 2009), and off the coast of North-west Africa (Krastel et al., 2019). Submarine slope failures mobilize large amounts of sediment from the continental margins toward the deep ocean and thus represent an important sediment transport mechanism (Hühnerbach & Masson, 2004). For comparison, the volume of material involved in the Storegga Slide has been determined at around 2,400–3,200 km³ (Haflidason et al., 2005), which greatly exceeds the volume of material involved, for instance, in the collapse of Mount St. Helens, which was estimated at around 2.8 km³ (Voight et al., 1983).

© 2022. The Authors.

This is an open access article under the terms of the [Creative Commons Attribution License](https://creativecommons.org/licenses/by/4.0/), which permits use, distribution and reproduction in any medium, provided the original work is properly cited.

Supervision: Morelia Urlaub, Christian Berndt

Validation: Thore F. Sager, Pauline Kaminski

Visualization: Thore F. Sager

Writing – original draft: Thore F. Sager, Morelia Urlaub, Christian Berndt

Writing – review & editing: Thore F. Sager, Morelia Urlaub, Pauline Kaminski, Galderic Lastras, Miquel Canals, Christian Berndt

Alongside the volume of material involved in slope failures and the runout velocity, the development of a slope failure determines its tsunamigenic potential (Harbitz et al., 2014; Lenz et al., 2018; Masson et al., 2006). For example, a multi-stage failure with long time periods in between individual stages is less tsunamigenic than a single event failure of the same mass (Harbitz et al., 2014). For assessing the tsunamigenic potential of a landslide, and thus the hazard it might represent, it is therefore essential to understand its detailed kinematic development and if possible, assess the volume of mobilized material.

Clare et al. (2019) reveal that ambiguity exists in the sound and consistent identification of morphometric parameters for submarine landslides. Whereas the length of evacuational and depositional zones, and the average slope angles are important input variables in predictive models for tsunamigenic potential of submarine landslides, errors in the identification of those tsunami source parameters may directly propagate into modeling results. Further, the retrogression of the headscarp needs to be addressed as it could indicate that the slope failure developed during several stages.

Previous studies based on bathymetric and 2D reflection seismic imagery provide valuable insights into landslide evolution (e.g., Barrett et al., 2020; Lenz et al., 2018). However, these data do not provide the three-dimensional structure of the entire submarine landslide. Therefore, a detailed analysis of various characteristics in and around submarine landslide deposits that are key to understanding emplacement processes, such as deformation of internal structure, distribution and size of transported blocks, erosion of underlying strata, or reconstruction of paleo-morphology has rarely been possible due to the lack of high-quality 3D reflection seismic data. Nonetheless, important work has been published on emplacement processes (e.g., Lenz et al., 2018; Steventon et al., 2019); deformation mechanisms (e.g., Ogata et al., 2014; Sobiesiak et al., 2018); transported blocks (e.g., Alves & Cartwright, 2009); erosive processes (e.g., Nugraha et al., 2020; Ogata et al., 2014; Sobiesiak et al., 2018); and reconstruction of the paleo seafloor morphology (e.g., Völker, 2010).

In this study, we use very-high resolution multibeam bathymetric and high-quality 3D reflection seismic reflection data, and re-processed high-quality 2D quality reflection seismic profiles that completely cover a small submarine landslide, named Ana Slide, located within the Eivissa Channel, Western Mediterranean Sea. Our objectives are to establish a relative chronology and reconstruct the kinematic development of Ana Slide. Our aim is to ameliorate current understanding on emplacement processes of submarine landslides, making use of the unique observational data base of Ana Slide.

2. Terminology

In this study, we use the term failure to describe the active process that translates or mobilizes landslide material from a source to a sink area. The resulting deposit is defined as the mass transport deposit (MTD) of Ana Slide. We refrain from the use of the classic terms of the “headwall” and “toe” domains. Although they correlate with the evacuational source and accumulative sink areas, they provide no information about kinematic processes involved in the emplacement and development of failure. Therefore, we use the terms “source” and “sink area” instead. While the source area can be identified from the upward deviation of contour-lines inside a landslide scar, the sink area will show downwards deviating contour-lines with respect to those of the surrounding seafloor. We also use the term by-pass zone to describe the transitional area in between the source and sink areas, where neither sediment has been removed nor added.

In addition, while the term MTD has previously been used to refer to all material involved in the slope failure (e.g., Bull et al., 2009; Frey-Martínez et al., 2005, 2006; Jackson, 2011; Lackey et al., 2018; Nugraha et al., 2020; Sobiesiak et al., 2016, 2018), we further distinguish between “landslide material” and “affected slope sediment.” The former describes material that was actively incorporated and mobilized during failure. The latter describes material that per se was not part of the landslide but experienced *in-situ* deformation immediately below mobilized landslide material.

By assuming that a slope failure did not change sedimentation patterns within the vicinity of a MTD, the top surface of a MTD is recognized as the boundary between relatively conformal reflections and chaotic/disrupted seismic facies within the MTD below (Bull et al., 2009).

The lower boundary with conformal seismic reflectors below is delimited by the “base of deformation” surface previously referred to as the “slip plane” or “glide plane” (Lastras et al., 2004). We use the term “basal shear

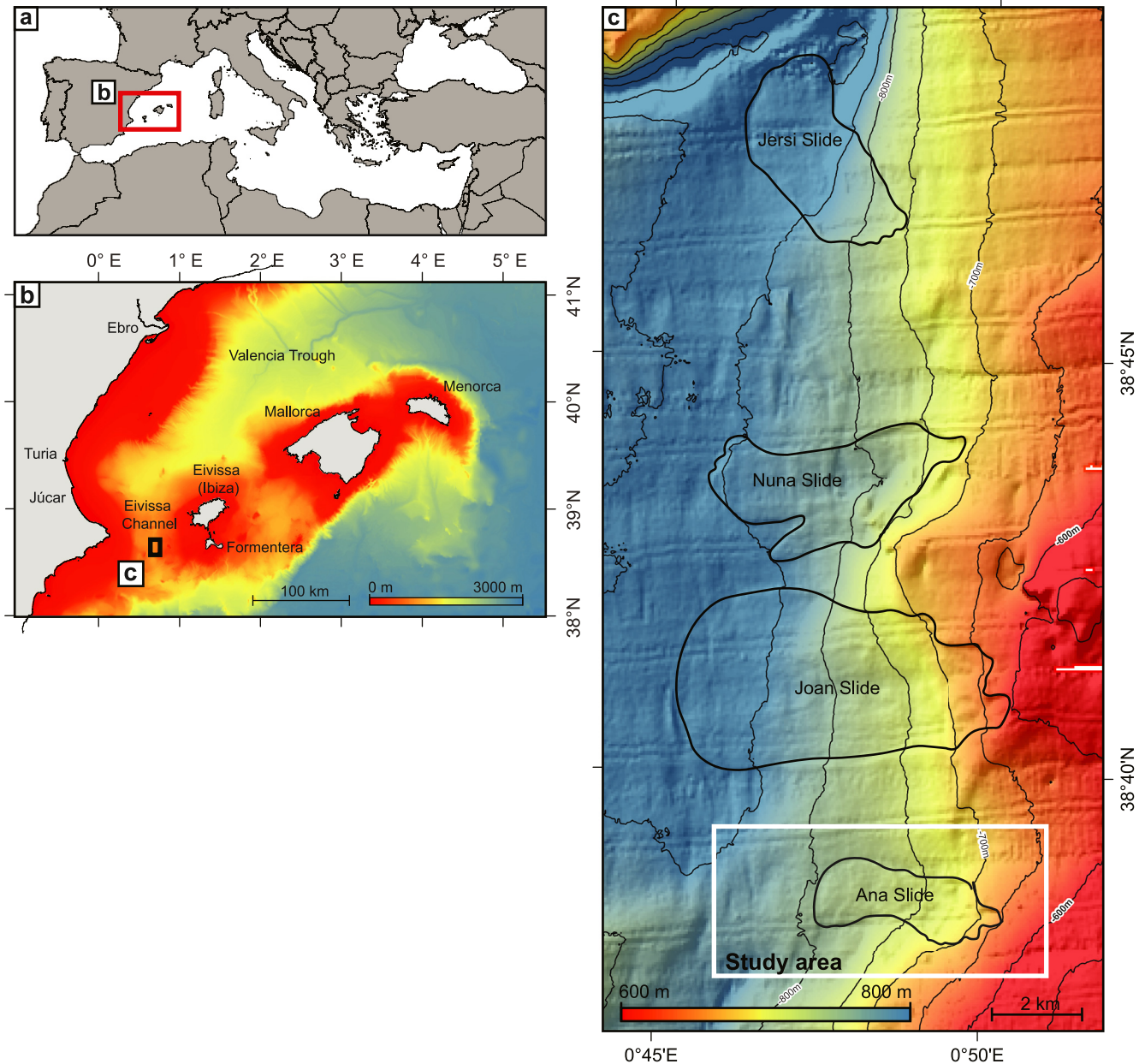


Figure 1. (a) Overview map of the Western Mediterranean Sea showing the location of the Balearic Promontory (BP). The red box indicates the location of panel b. (b) General bathymetric map of the Balearic Promontory. Data from the “Global multi-resolution topography synthesis” (Ryan et al., 2009). The black box indicates the location of panel c. (c) Bathymetric map of the eastern slopes of the Eivissa Channel showing the outlines of Jersi, Nuna, Joan, and Ana Slides. Bathymetric data from the BIG’95 survey. The white box indicates the location of the study area (Figure 2).

surface” to describe the interface between mobilized landslide material from affected slope sediment below. In this study we expand on the classical usage of “seismic stratigraphy” (Mitchum et al., 1977). In addition to seismic reflectors having a chronological significance that bound seismic units, we introduce several sub-units bound by the same seismic reflectors that reflect for instance *in-situ* deformation of parts of the unit.

3. Geological Background and Previous Studies

The Eivissa Channel is located at the western end of the Balearic Promontory (Figure 1). It includes the islands of Eivissa (Ibiza) and Formentera, Mallorca, and Menorca, from west to east. The Promontory is the north-eastern prolongation of the Betic Range that extends along the southern Iberian Peninsula (Maillard & Mauffret, 2013;

Mauffret et al., 1995). The regional structural framework is controlled by strong compressive activity that initiated in the Late Oligocene. Contraction was completed during the Serravalian and since then the Balearic Promontory has experienced extension (Maillard & Mauffret, 2013). Hence, the Promontory is located in a complex setting with successive compression and extension phases, though at present it shows relatively little tectonic activity (*sensu del Valle et al.*, 2016).

From short 3–6 m long gravity cores, local sediments in the Eivissa Channel are identified as carbonate-rich (~50% CaCO₃) silty clays (~60% clay and ~30% silt) with biogenic sands (~10%) with limited organic content (TOC <0.5%) (Lafuerza et al., 2012; Panieri et al., 2012). Siliciclastic input into the Eivissa Channel is limited, clayey, and originates from rivers such as the Ebro, Turia and Júcar on the Iberian Peninsula, north-west of the study area (Panieri et al., 2012). Hence, low accumulation rate, fine-grained hemipelagic carbonate-rich sedimentation dominates the study area (Canals & Ballesteros, 1997).

Previous studies evaluated failures within the Eivissa Channel by means of geophysical data sets (Berndt et al., 2012; Lastras et al., 2004, 2006), gravity cores (Panieri et al., 2012) and in combination with geotechnical CPTu measurements (Lafuerza et al., 2012). Lastras et al. (2004, 2006) identified three additional MTDs north of Ana Slide called Joan, Nuna, and Jersi from south to north (Figure 1). Ana Slide is located at water depths between 630 m to the east and 790 m to the west (Figure 2). It has a maximum length from east to west of 4.1 km with a headscarp height of ~30 m while the average slope angle is ~2° (Figure 2).

In 2006, the RSS Charles Darwin Cruise 178 acquired high-resolution bathymetric and 3D seismic reflection data. From these, a buried slope failure—pre-Ana Slide—was mapped in detail around 30–40 ms travel time below Ana Slide (Berndt et al., 2012). While pre-Ana Slide extends around 1.4 km westwards of Ana Slide the shape and location of the headscarps are very similar (Figure 2).

Lastras et al. (2004) propose that fluid overpressure indicated by the presence of fluid escape structures in the vicinity of Ana Slide and mechanically weak layers are the main controlling factors for slope failures along the eastern slope of the Eivissa Channel. In addition, they indicate that failures throughout the Eivissa Channel possibly occurred simultaneously as they share the same seismic horizon—the “slip plane”—as their basal shear surfaces. The study by Lafuerza et al. (2012) corroborates this by geotechnical tests on Kullenberg piston core samples and *in-situ* CPTu measurements, while adding that failure required the presence of gas in the substrate. Cattaneo et al. (2011), using AMS radiocarbon dating, planktonic foraminiferal assemblages, and correlation with regional oxygen isotope curves, suggest an age of ~61.5 ka. B.P. for Ana Slide. Berndt et al. (2012) propose, from the analysis of a 3D reflection seismic data, that both slides were caused by changes of pore pressure as indicated by the spatial relation between pre-Ana and Ana Slide and by evidence for gas and fluid migration. Panieri et al. (2012), based on δ¹³C benthic foraminifera records, show that methane was released from the seabed before and during the failure of Ana Slide.

Although these previous studies regard the physiography and potential triggering, the internal architecture of Ana Slide and its complete kinematic development has yet to be addressed from analysis of 3D reflection seismic data. Hence, within this study, the kinematic development of Ana Slide is presented, which lends itself as a natural laboratory for more extensive landslides that are not fully covered by bathymetric or reflection seismic data.

4. Data and Methodology

The 3D reflection seismic data were acquired with the P-Cable system of the National Oceanographic Centre, Southampton, UK during cruise CD178 in 2006 onboard the RRS Charles Darwin alongside a high-resolution bathymetric grid (Berndt et al., 2012). Additional bathymetric data acquired during cruise BIG'95 in 1995 onboard R/V Hespérides (50 m grid spacing) are also considered (Figure 1c) (Lastras et al., 2004).

The P-Cable system consisted of two paravanes and a central buoy, spanning a perpendicular cable. From this cable we towed eleven 12.5 m-long single-channel Teledyne streamers (Berndt et al., 2012). The seismic source consisted of four 40 in³ Bolt 600B airguns spaced 0.75 m apart, towed at a depth of 1.5 m about 20 m behind the vessel. The processing steps for the 3D reflection seismic data included frequency filtering (35–350 Hz) before a 3D Stolt time migration with a migration velocity of 1,500 m/s was applied (Berndt et al., 2012). The data have an inline and crossline spacing of 10 m. Given the high frequency of the 3D reflection seismic data the vertical seismic resolution, defined as 1/4 of the dominant wavelength, is approximately 5–6 m immediately beneath the

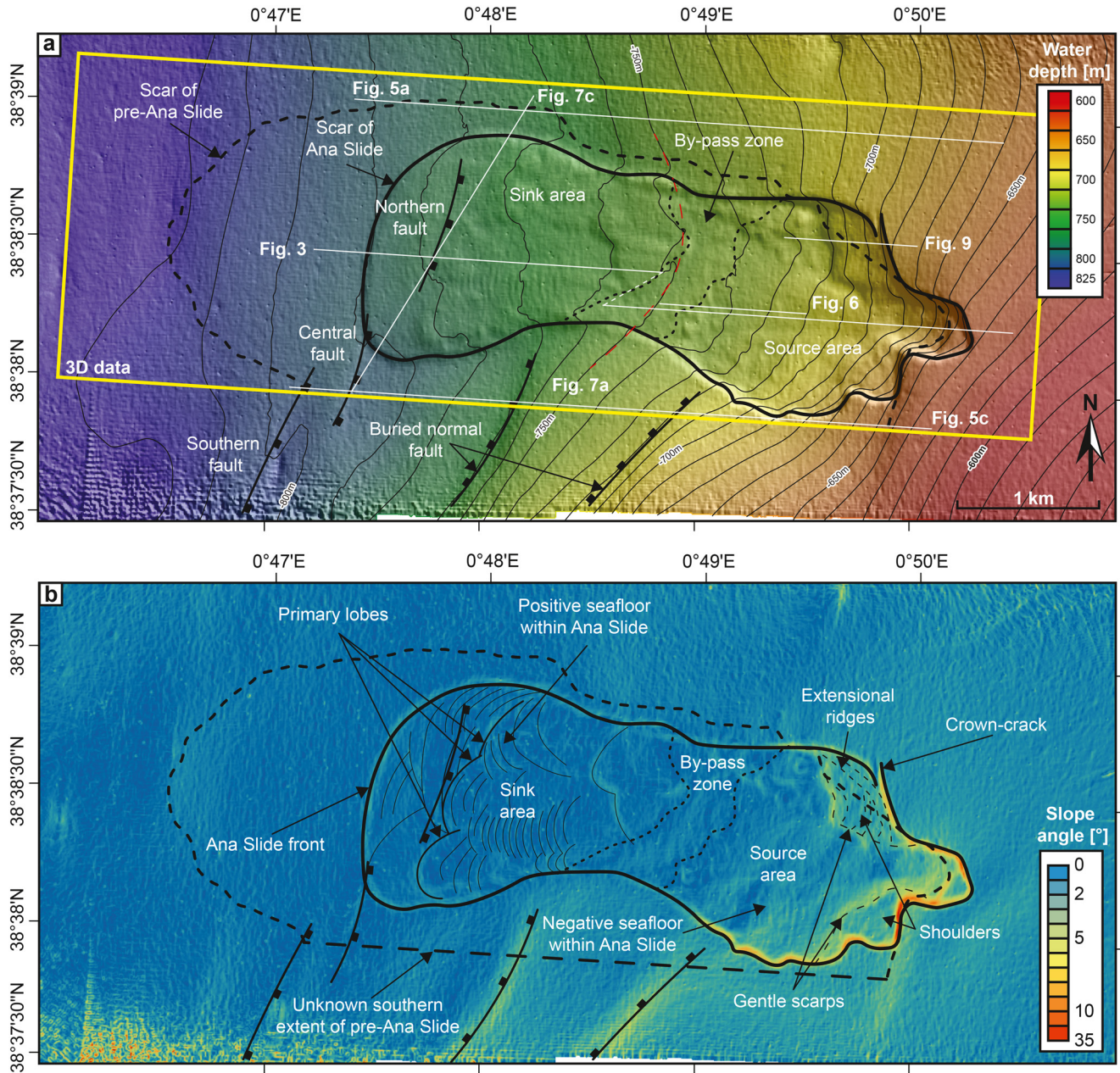


Figure 2. (a) Detailed bathymetric map of the study area with 10 m contour-line spacing. Ana Slide is outlined by a solid black line, while the outline of pre-Ana Slide is highlighted by a stippled black line. The location of reflection seismic profiles in subsequent figures is shown with solid white lines. Inside Ana Slide, the 750 m contour-line corresponds to those interpolated from outside Ana Slide (stippled red line). Several seafloor offsetting features are located south off and below the downslope part of Ana Slide. (b) Slope gradient map of the study area. Kinematic features are highlighted. The seafloor is gentle outside and north of Ana Slide while toward the south the seafloor displays several offsetting features.

seafloor ($V_p = 1,500$ m/s). The data are displayed in the way that a downward increase in acoustic impedance is represented by a red-blue-red wavelet (e.g., Figure 3).

For bathymetric analysis we used the ArcGIS (ArcMAP) 10.6 software. Interpretation of the reflection seismic data and further data integration was carried out in IHS KingdomSuite 2018/2020. We calculated the *Smoothed Dip of Maximum Similarity* attribute on the SFR reflector from the *RockSolid Attributes* to map lateral discontinuities.

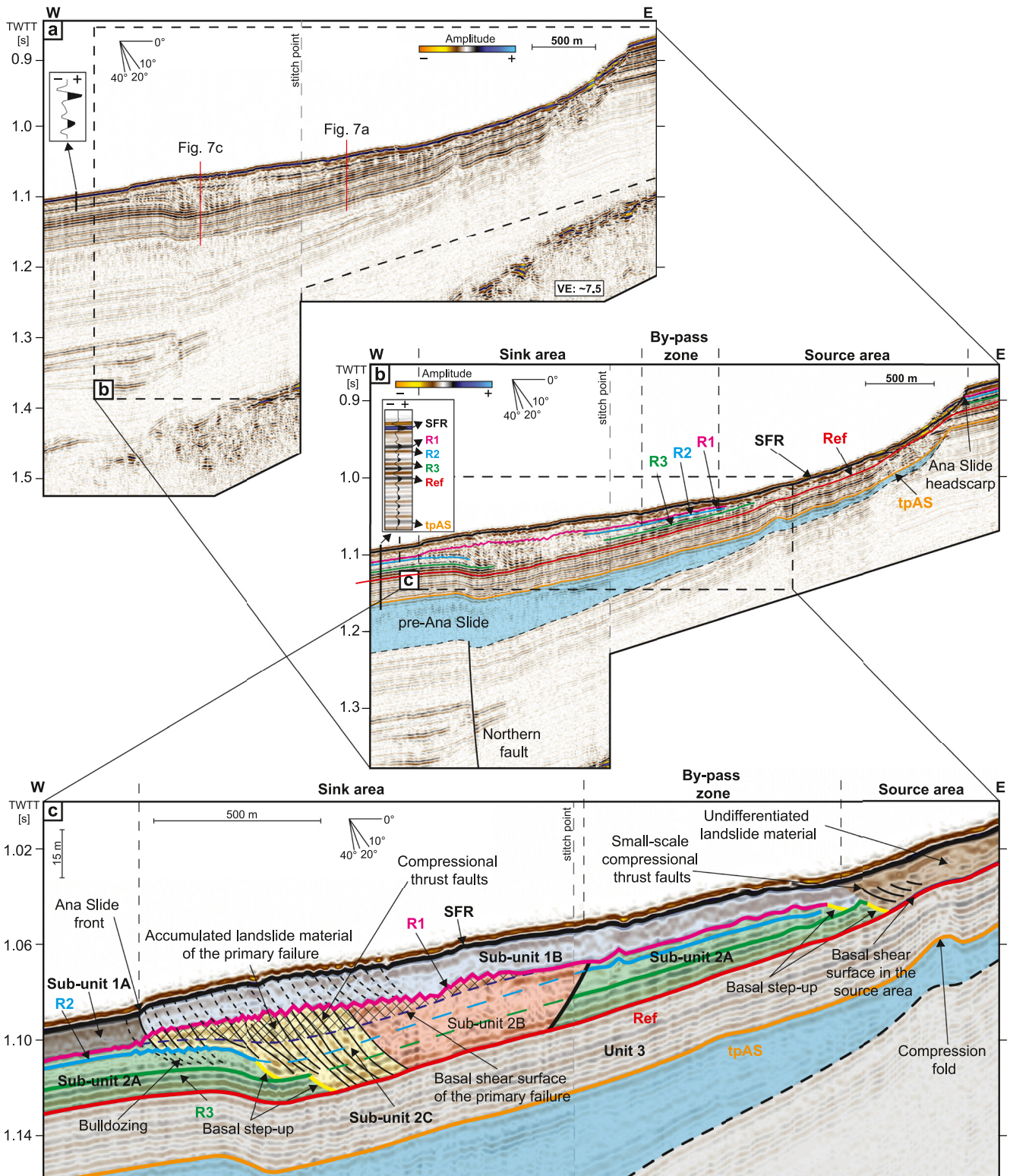


Figure 3. (a) Uninterpreted stitched reflection seismic profile (re-processed 2D data) through Ana Slide (Figure 2). The combination of two profiles shows the Ana Slide represented along-strike through the source and sink areas. (b) Close-up of Ana Slide with interpretation of key seismic reflectors: SFR, R1, R2, R3, Ref, and tpAS. (c) Sketch of seismic units. Sub-units involved in Ana Slide are 2B, 2C, 1B, and undifferentiated landslide material. Sub-units 2A and 1A characterize un-affected slope sediments outside the scar of Ana Slide. A compression fold that affects tpAS is located toward the east at depth while the basal shear surface inside the source area is represented by Ref. A visual comparison of the 3D and 2D reflection seismic profiles is presented in Figures S6–S11 of Supporting Information S1.

4.1. Additional Seismic Processing

For this study, we re-analyzed the 3D reflection seismic data because they are affected by receiver ghosts (e.g., Figure 7) and identified the cables that were affected by receiver ghosts. These receiver ghosts were generated by varying streamer depths during seismic acquisition as the perpendicular cable apparently sagged between the paravanes and the central buoy. Streamers close to the paravanes and the central buoy show little receiver ghosts. For the detailed analysis we extracted only the 2D profiles along the streamers that were not affected by the receiver ghost. Obviously, this higher resolution was bought at the expense of incomplete coverage. A visual comparison between profiles from the 3D data and re-processed 2D profiles is provided in Figures S6–S11 of Supporting Information S1 and location of profiles (S5). In the figures we normally present the single-channel 2D reflection seismic profiles extracted from inlines unaffected by the receiver ghost, while plan view maps of key seismic horizons and seismic attributes are derived from the binned 3D reflection seismic data set which is partly affected by receiver ghosts (Table S1 in Supporting Information S1). The extracted 2D profiles are frequency bandpass filtered and burst noise attenuated. These data were binned, NMO-corrected, and stacked. Finally, a Stolt migration with seismic velocities of 1,520 m/s was applied.

The receiver ghosts affect the entire traces in the 3D reflection seismic data set. As they only occur on individual streamers that are too deep below the surface, they align with the ship track. This makes their identification fairly easy in map view as they appear as stripes on attribute map. These have not been used for interpretation. For depth conversion of Ref and R1 we used seismic velocities of 1,500 m/s and volume calculation was performed inside the sink area.

The “Smoothed Dip of Maximum Similarity” attribute is derived from a similarity attribute. First semblance between adjacent traces is calculated for a moving window. Then, the dip is calculated for the maximum semblance direction, and this is smoothed spatially. The Smoothed Dip of Maximum Similarity attribute is able to highlight the depositional environment and detect faults. These faults are representative of compressional ridges, extensional normal faults, ridges, and the front of Ana Slide that are characterized as structural elements namely faults.

5. Results

5.1. Morphology of Ana Slide

Ana Slide is located on the eastern slopes of Eivissa Channel (Figure 1). The surrounding seafloor is gently inclined from east to west and relatively smooth immediately north of Ana Slide while several seafloor offsetting features are located along its southern vicinity (Figure 2). The upslope scar of Ana Slide referred to as the head-scarp is cauli-flower shaped meaning that it consists of several smaller headscarp sections upslope. The landslide is 1.5 km wide from north to south. The headscarp forms two distinct “shoulders,” with the southern shoulder being steeper than the northern one. These shoulders, in turn, have gentle scarps ($<10^\circ$) located some hundreds of meters downslope (Figure 2). Around 1.5 km downslope of the headscarp, the sidewalls form a narrow, approximately 1.1 km wide corridor with irregular seafloor morphology.

The frontal break of slope that marks the downslope-most extent of Ana Slide opens to around 1.5 km width. In this study we refer to it as the “front of Ana Slide.” Inside this lower part we identify three primary lobes located around 300–500 m upslope of the front of Ana Slide. The primary lobes are visible in the slope map as minor ($2\text{--}4^\circ$) concave downslope breaks of slope and show numerous pressure ridges (Figure 2). These ridges align approximately parallel to the front of Ana Slide. In the northern downslope part, Ana Slide is around 5 m higher with respect to the surrounding seafloor outside the scar of Ana Slide while this difference is less significant in the southern downslope part.

5.2. 3D Seismic Interpretation

For the analysis of the kinematic development of Ana Slide we mapped five key seismic reflectors (Figure 3). These were mapped in both the 3D and 2D reflection seismic data and used accordingly to the data presented.

5.2.1. Reference Reflector (Ref)

The high-amplitude positive regional Reference (Ref) reflector (marked in red) is present throughout the study area (Figure 3). Inside the scar of Ana Slide it correlates with the apparent slip plane reflector identified by

Lastras et al. (2004). This reflector is the shallowest undisturbed stratigraphic reflector throughout Ana Slide. While in some places, such as the upslope eastern part of the slide, it indeed represents the slip plane, in other areas it is overlain by undisturbed and disturbed reflections. Thus, it is an important reference surface for the further discussion of the slide's thickness variations.

5.2.2. R3 and R2 Reflectors

The moderate-amplitude negative R3 and R2 (marked in green and light-blue) are mapped around 10 and 20 ms above Ref (Figure 3). Within the upslope part both reflectors are absent to around 1.5 km downslope of the easternmost headscarp. The lateral extent of R3 is limited to a small circular region with a diameter of around 500 m located within the central lower part approximately 900 m upslope of the front of Ana Slide (Figure 4). In contrast, R2 extends around 300–500 m upslope of the front of Ana Slide. In profile, R3 is irregular while R2 exhibits a strong hummocky appearance toward the front of Ana Slide (Figure 3) while both R2 and R3 have a congruent upslope extent.

5.2.3. R1 Reflector

R1 reflector (marked in pink) is the first high-amplitude positive reflector beneath the Seafloor (SFR) reflector (Figure 3). It is absent within the upslope part of the landslide to around 1.5 km downslope of the headscarp. The upslope limit of R1 is congruent with that of R2 and R3 and parallel with Ref for around 500 m downslope. It appears irregular within the lower area, while outside the scar of Ana Slide reflections are continuous and parallel with R3, R2, and Ref.

5.2.4. Seafloor or Ana Slide Top Reflector (SFR)

The very-high-amplitude positive Seafloor reflector (SFR) (marked in black) represents the seafloor and the assumed top Ana Slide reflector since they cannot be distinguished due to limited vertical resolution (Figure 3). Hemipelagic sediment deposited after the Ana Slide failure that was identified in sediment cores (2.5 m) by Cattaneo et al. (2011) and Lafuerza et al. (2012) is, consequently, included.

5.2.5. Top pre-Ana Slide Reflector (tpAS)

The top pre-Ana Slide (tpAS) reflector (marked in orange) is the upper reflector of pre-Ana Slide (Figure 3). It separates chaotic reflections below, which correspond to material of pre-Ana Slide with conformal reflections above up to 40 ms below Ref.

5.3. Seismic Units

Within this study, we define three seismic units according to their seismic facies, relation to Ana Slide, and lateral extent bound by reflectors. These seismic units are sub-divided into several sub-units: 2A, 2B, 2C, 1A, and 1B. Throughout the study area such as immediately west of Ana Slide (Figure 3) the reflectors that bound these units are conformally arranged and highlight that sedimentation was relatively steady since before the emplacement of pre-Ana Slide (Panieri et al., 2012). Nonetheless, these sediments have probably been deposited at an unsteady pace in response to eustatic or climatic changes throughout the Quaternary but were relatively unaffected by other processes such as contour-currents.

5.3.1. Unit 1

This unit appears between R1 and SFR (Figure 3) and was mapped from the re-processed 2D reflection seismic data. The isochron map of Unit 1 is presented in Figure 4a. Unit 1 is sub-divided into sub-units 1A and 1B. Sub-unit 1A is located outside the scar of Ana Slide and consists of conformal and continuous reflectors arranged in a slight downslope thickening configuration (Figure 4a). Sub-unit 1B is made of moderate-amplitude, highly irregular and disrupted reflections within the scar of Ana Slide. Unit 1 is absent within the upslope part of Ana Slide, while it is composed of slope sediment that was present within the lower part and landslide material that accumulated during the secondary failure. The isochron map of Unit 1 shows distinct ridges orientated sub-parallel toward the front of Ana Slide (Figure 4a).

5.3.2. Unit 2

This unit occurs between Ref and R1 (Figure 3c) and was mapped from the 3D reflection seismic data. The isochron map of Unit 2 is presented in Figure 4b. Unit 2 is sub-divided into three sub-units. Sub-unit 2A, formed

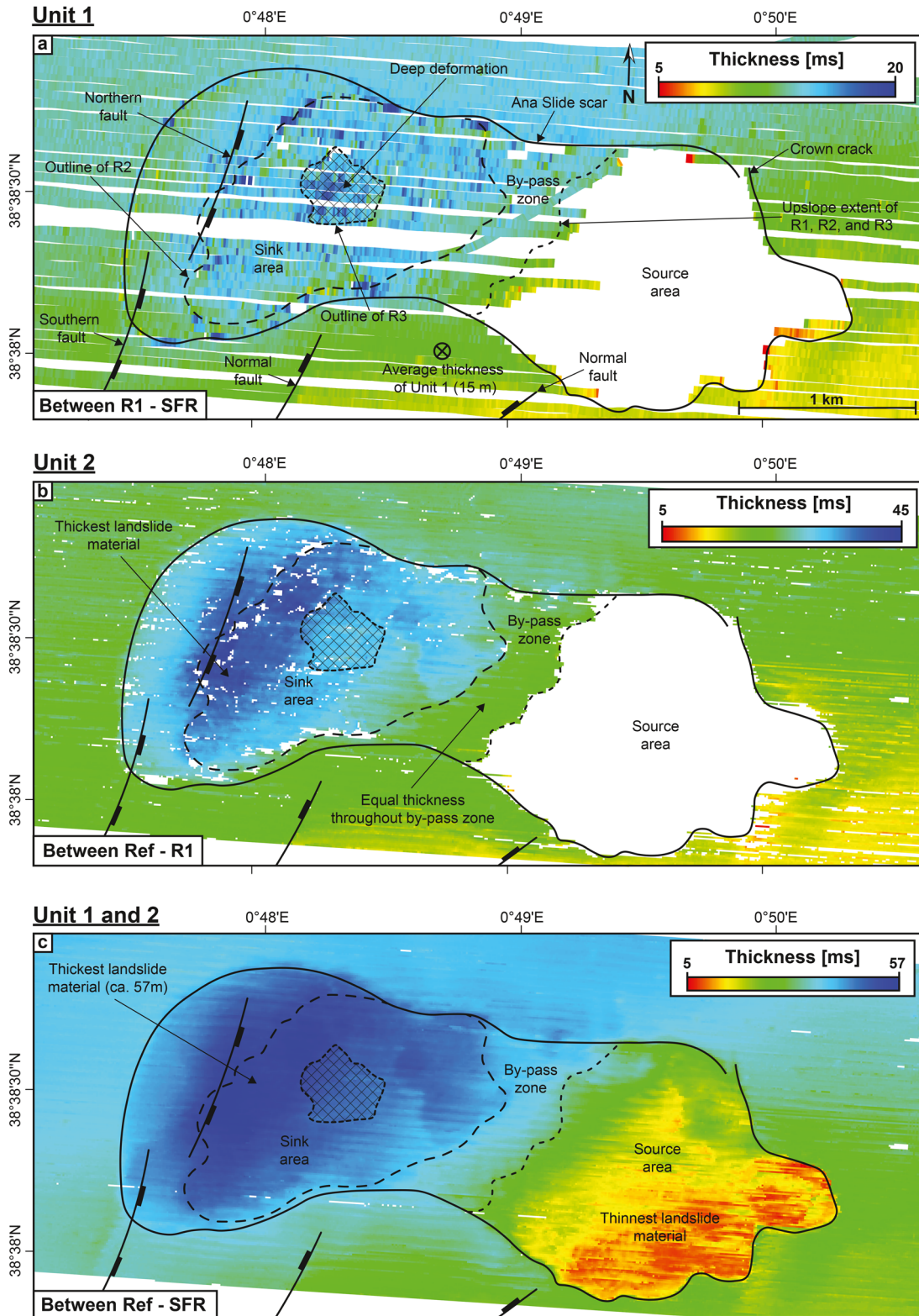


Figure 4.

by high-amplitude continuous parallel seismic reflections located primarily outside the scar of Ana Slide in a downslope thickening configuration (Figure 4b). Sub-unit 2A is present within the scar of Ana Slide in an area around 500 m downslope of the upslope limits of R3, R2 and R1 (Figure 4b). Inside the scar of Ana Slide Sub-unit 2B generally describes chaotic seismic facies with lower-amplitude, highly disrupted reflectors, while Sub-unit 2C displays semi-continuous, moderately higher-amplitude disrupted reflectors. The lateral extent of these sub-units is sketched in Figures 4a–4c and the isochron map of Unit 2 is shown in Figure 4b. Unit 2 is thickest in the downslope part of Ana Slide about 300–500 m upslope of the front of Ana Slide. Outside the scar of Ana Slide, the thickness increases linearly in downslope direction.

5.3.3. Unit 3

This unit is located below Ref (Figure 3). It includes the interval between pre-Ana and Ana Slide, material of pre-Ana Slide, and all material below. For instance, between Ref and tpAS reflections are conformal and characterize a steady hemipelagic depositional environment.

5.3.4. Undifferentiated Landslide Material

This unit occurs above Ref and around 1.5 km downslope of the headscarp (Figure 3). It characterizes disrupted, lower-amplitude seismic reflections. This unit could not clearly be associated with Sub-unit 1B, 2B or 2C. It represents material that was involved in Ana Slide that cannot be distinguished conclusively.

5.4. Faults and Crown-Cracks

Several faults are identified within the study area from both bathymetry and reflection seismic data (Figure 2). These are primarily located along the southern vicinity of Ana Slide (Figures 5c and 5d). There are two faults that dip down-slope that is, westwards, and three faults that dip eastwards. All strike in NNE-SSW direction. Two of the three eastwards inclined faults are covered by reflection seismic data (Figure 2). These three faults characterize an en-echelon fault system of unknown southwards extent that terminates to the north below the downslope part of Ana Slide. In addition, a crown-crack exists immediately upslope north-east of the headscarp that detaches northwards. Within Ana Slide, numerous small-scale compressional thrust faults terminate from Ref up to R1 (e.g., Figures 3 and 6). Some thrust faults located around 500 m upslope of the front of Ana Slide reach SFR (e.g., Figure 3). Upslope the extents of R2 and R3 small-scale compressional thrust faults are identified in profile (Figure 6).

5.5. MTD Kinematic Domains

5.5.1. Source Area

By comparing the shape and orientation of the present-day contour lines with those interpolated from outside the scar of Ana Slide and into the slide area (Figure 2), the evacuational source area is defined by the downwards excursion of present-day bathymetric contours (representing loss of material). This area extends around 1.5 km downslope of the easternmost headscarp and is congruent with the upslope limits of R3, R2, and R1 (Figures 3 and 4). Within the source area, the thickness of Ana Slide is defined by the interval between Ref and SFR or units 1 and 2 and here the source area thickness is significantly thinner compared to outside the scar of Ana Slide and thus the source area was not completely evacuated. Immediately upslope of the by-pass zone the remaining landslide material experienced shortening, as evidenced by small-scale compressional thrust faults (e.g., Figure 6).

The isochron map of Ref—SFR is thickest in the western part of the source area and thinnest in the south-eastern part (Figure 4c). In particular, on the northern shoulder, the interval between Ref-SFR is almost twice as thick as on the southern shoulder.

Figure 4. Isochore maps of units 1 and 2. (a) Thickness of material between R1—SFR that represents Unit 1 (re-processed 2D data). “Average thickness of Unit 1” is approximately 15 m using a seismic velocity of 1,500 m/s for depth conversion. Ref is absent inside the source area and no isochore map was calculated inside this area. (b) Thickness of material between Ref—R1 that represents Unit 2 (3D data). Receiver ghosts are introduced into the 3D reflection seismic data from varying streamer depth during seismic acquisition. The thickest landslide material is located within the central sink area immediately upslope of the northern fault with *in-situ* deformation located some hundreds of meters upslope of thickest landslide material. Ref is absent inside the source area and no isochore map was calculated inside this area. (c) Thickness of material between Ref—SFR represents both units 1 and 2 (3D data). The southern, central, and eastern source area are significantly thinner than the area along the north-eastern headscarp. Material is thickest (ca. 43 m) within the central and along the northern sink area and upslope of the northern fault.

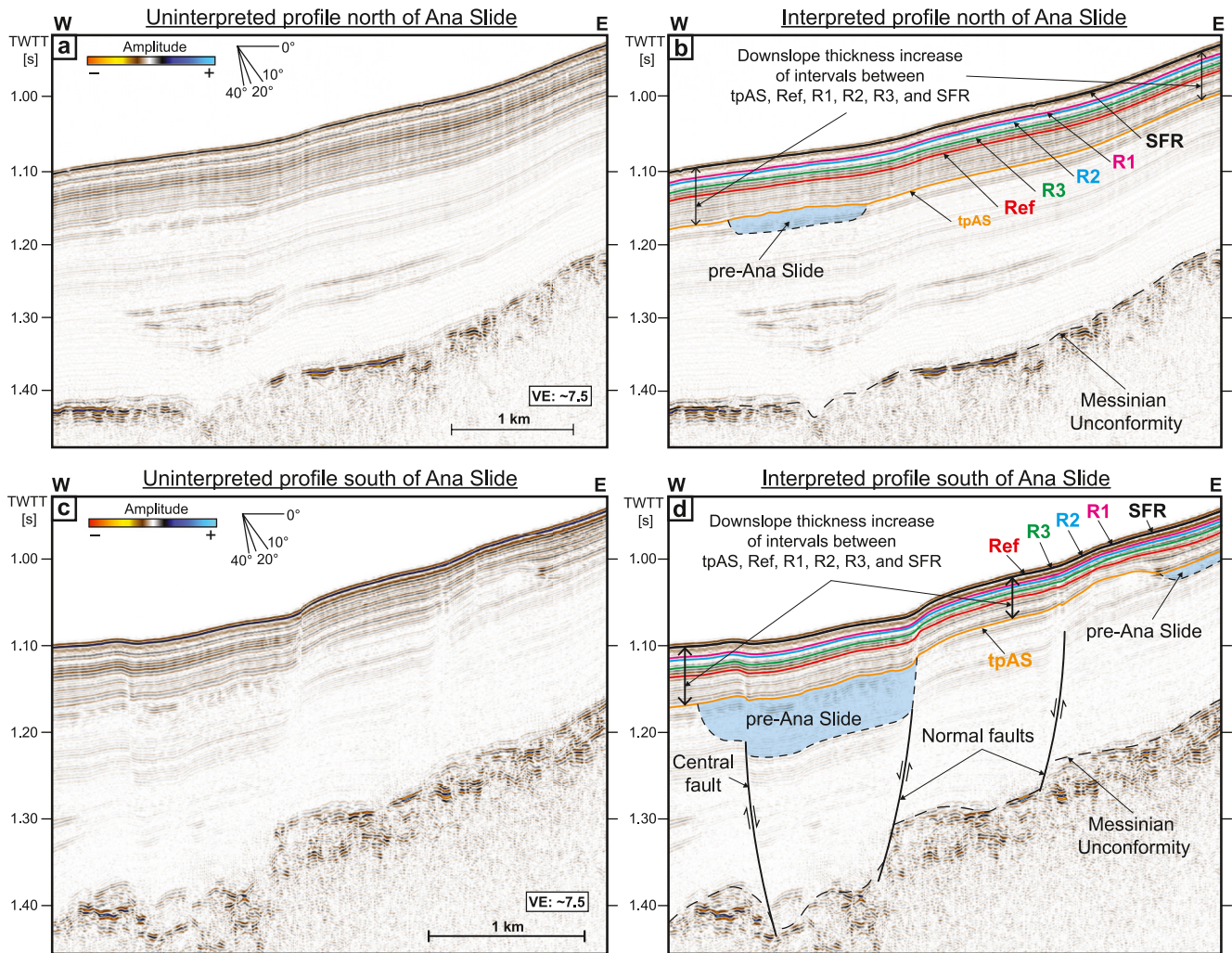


Figure 5. (a) Un-interpreted profile (re-processed 2D data) north of Ana Slide (see location in Figure 2). (b) Interpreted profile (re-processed 2D data) north of Ana Slide. The intervals between SFR, R1, R2, R3 and Ref thicken in downslope direction representing Unit 2 (Ref-R1) and Unit 1 (R1-SFR). (c) Un-interpreted profile (re-processed 2D data) south of Ana Slide (see location in Figure 2). (d) Interpreted profile (re-processed 2D data) south of Ana Slide. The intervals between SFR, R1, R2, R3, and Ref thicken in downslope direction representing Unit 2 (Ref-R1) and Unit 1 (R1-SFR) but are locally controlled by the recent activity of normal faults and the central fault. A visual comparison of the 3D and 2D reflection seismic profiles is presented in Figures S6–S11 of Supporting Information S1.

5.5.2. Transitional Domain or “By-Pass Zone”

For Ana Slide the bathymetry shows no significant deviation from the 750 m contour line where the scar of Ana Slide narrows (Figure 2) that we define as the transitional domain or more accurate for this study the by-pass zone. It indicates either that no material has been added or removed by the landslide, or that the removed material has been replaced by material coming from the source area with no thickness variation. The zone representing the by-pass zone extends over a downslope distance of about 500 m from approximately 700 to 800 m water depth and coincides with the narrowing of the scar of Ana Slide. The upslope extent of the by-pass zone coincides with the upslope termination of R3, R2 and R1 (Figures 4a–4c and 6b).

The reflection seismic data provide insight into the kinematics of the by-pass zone. Seismic coherent reflections of Sub-unit 2A above Ref up to R1 (Figure 3) continue uninterrupted out of the scar of Ana Slide (Figures 7a and 7b). The isochron maps between Ref—R1, R1—SFR, and Ref—SFR show equal thickness throughout the by-pass zone and the surrounding areas toward the north and south (Figure 4). These observations suggest that the by-pass zone is intact in its entirety and that it was not moved at depth between Ref and R1. We would expect to see at least some disruption of the seismic reflections if the by-pass zone had been translated, moved, or affected

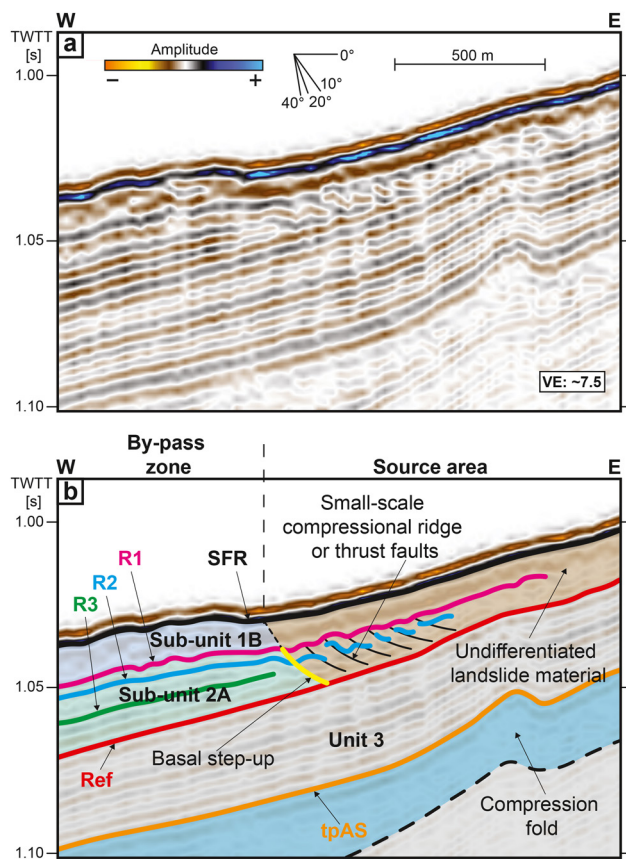


Figure 6. (a) Un-interpreted profile (re-processed 2D data) through the by-pass zone (see location in Figure 2). (b) Interpreted profile showing small-scale compressional ridges that are located within undifferentiated landslide material immediately upslope of the by-pass zone. A basal step-up exists downslope of the small-scale compressional ridges and material that composes the by-pass zone. A visual comparison of the 3D and 2D reflection seismic profiles is presented in Figures S6–S11 of Supporting Information S1.

area, mobilized on R1 through the by-pass zone and deposited within the sink area, forming parts of Sub-unit 1B. Hence, Sub-Unit 1B is the sum of *in-situ* Sub-Unit 1A and failed and mobilized Sub-Unit 1A (originating from the source area).

Sub-unit 1B lies above material that was previously deposited within the sink area (Figures 3b, 3c, 7c, and 7d) and R1 separates it from the underlying sediments. This previously deposited material relates to Unit 2 located between Ref and R1 that is significantly thickened toward the central sink area immediately upslope of the northern fault (Figure 4b). In addition, R1 has a strongly irregular appearance in the sink area (Figures 3b and 3c), which we interpret to represent the top surface of an earlier stage of failure. Hence, Sub-unit 1B depicts a failure that is stratigraphically separated from underlying material beneath R1. The fact that (a) Unit 1 has constant thickness between R1 and SFR outside the scar of Ana Slide, (b) Unit 1 is practically absent in the source area, and (c) R1 separates Unit 1 and Unit 2, indicates that landslide material of sub-units 2B and 2C must have moved prior to deposition and failure of Unit 1. Hence, contrarily to the interpretation of Lastras et al. (2004), Ana Slide comprises two failure events. These are separated in time by the period it took to deposit Unit 1. We call these two events the “primary failure” and the “secondary failure.”

Based on a 2–3 m thick post-failure drape, Cattaneo et al. (2011) inferred that Ana Slide occurred approximately 61.5 ka B.P. Following our interpretation, this age corresponds to the occurrence time of the secondary failure. The age proposed by Cattaneo et al. (2011) assumes an average sedimentation rate of around 5 cm/ka for the study area. From the reflection seismic data, we infer an average thickness of Unit 1 of about 15 m, using seismic

by the mobilization of landslide material below R1 and therefore the by-pass zone not been part of the failure process.

5.5.3. Sink Area

In the sink area Ref marks the lowest stratigraphic level of observed deformation. Within the sink area the *in-situ* deformation zone is marked by the lateral extent of R3 (Figure 4). Toward the front of Ana Slide *in-situ* deformation steps up stratigraphically from Ref to R3, R2, and R1 (Figure 3).

The isochron map of Ref—SFR shows thickness variations throughout the sink area (Figure 4c). The maximum thickness of 57 ms TWTT (ca. 43 m) occurs around 300–500 m upslope of the front of Ana Slide. The isochron map shows a depositional center immediately east of the northern fault that extends toward the northern scar of Ana Slide within the sink area (Figures 4b and 4c). From there, thickness in the interval between Ref—SFR and Ref—R1 decreases gradually to the south and east. The volume of Sub-unit 2B and 2C meaning the material involved in landsliding inside the sink area is 0.058 km³.

6. Discussion

6.1. Chronology of Ana Slide

Reflection seismic data allow constraining the relative temporal development of the failure of Ana Slide, the timing of which is poorly constrained in terms of absolute dates (e.g., Cattaneo et al., 2011). The lateral continuity of reflectors and the constant thickness of units outside the scar of Ana Slide indicate that units 1, 2, and 3 have been deposited by relatively steady hemipelagic sedimentation and only within Ana Slide are they reworked by gravity processes (e.g., Figures 3, 4c, and 5). Of these, the failure of Ana Slide involved units 1 and 2.

Unit 1 shows slight thickness variations toward the west and immediately north of Ana Slide (Figure 4a). Within the source area, though barely present, Unit 1 is partly represented by undifferentiated landslide material. Inside the scar of Ana Slide Unit 1 is thicker within the sink area compared to outside of it. We thus infer that material of Sub-unit 1A was evacuated from the source

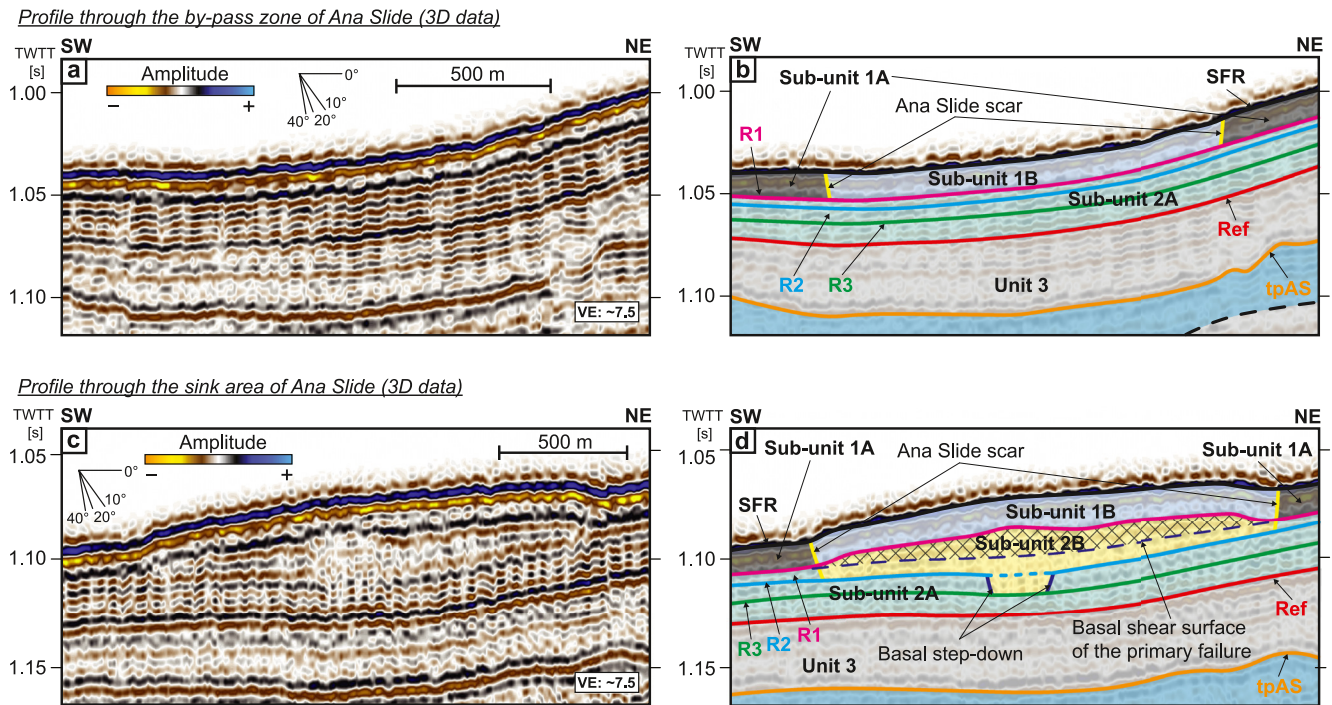


Figure 7. Transect profiles through the by-pass zone and sink area of Ana Slide. (a) Uninterpreted transect profile (3D reflection seismic data) through the by-pass zone of Ana Slide (see location in Figures 2 and 3). 3D reflection seismic profiles on crosslines show receiver ghost as continuous irregularities throughout both profiles (a and c). (b) Interpreted transect profile through the by-pass zone of Ana Slide. Material of Sub-unit 1B is located above un-affected and *in-situ* slope sediment of Sub-Unit 2a. The outline and scar of Ana Slide is highlighted by solid yellow lines. Note the lack of thickness variation within Ana Slide of units 1 and 2 compared to outside of Ana Slide. (c) Uninterpreted transect profile (3D reflection seismic data) through the sink area of Ana Slide (see location in Figures 2 and 3). (d) Interpreted transect profile through the sink area of Ana Slide. Material of Sub-unit 2B is significantly thickened within the sink area and extends into material of Sub-unit 2A below. The hatched area represents accumulated landslide material within the sink area. Here, material inside Ana Slide is significantly thickened compared to outside of Ana Slide between Ref and SFR namely by the thickness of Sub-unit 2B.

velocities of 1,500 m/s (Figure 4a). Assuming no change in sedimentation rate, this would result in a time-lag between the primary and secondary failure of approximately 300 ka. This is a very rough estimate because it is likely that sedimentation rates throughout the Eivissa Channel varied due to sea-level oscillations during the late-Quaternary linked to climate variability (Hodge et al., 2008; Tuccimei et al., 2007) and that the seismic velocities are poorly constrained for the study area with the exception of velocities measured from a shallow gravity core (Lafuerza et al., 2012) (Figure 2).

6.2. Headscarp Retrogression During the Primary and Secondary Failures

The headscarp of Ana Slide is characterized by multiple smaller headscarps linked with “shoulders” in the northern and southern source area (Figure 2). The slide plane steps up stratigraphically forming terraces. Each of these terraces has its own headscarp and the shape of the overall headscarp is comprised of these individual segments resulting in a cauliflower-shape, which has been shown as typical morphology for retrogressive landslide behavior (Micallef et al., 2008). The observation of at least two shoulders therefore suggests that the present-day headscarp of Ana Slide formed by multiple failures and retrogression. In addition, the relative position and size of the Ana Slide headscarp segments suggest that the failures associated with retrogression involved smaller amounts of material during successive failure. It is not possible to relate individual headscarp segments to the primary and secondary failures discussed above.

We observe a crown-crack along the northern headscarp of Ana Slide (Figure 2). Here within the northern source the slope gradient is gentler compared to that within the central and southern source areas (Figure 2). Crown-cracks have been described to form as a result of extensional stresses related to upslope propagating retrogressive failures (Frey-Martinez et al., 2005; Varnes, 1978). We therefore interpret that this crown-crack was generated by latest headscarp retrogression, because material within the northern source area immediately

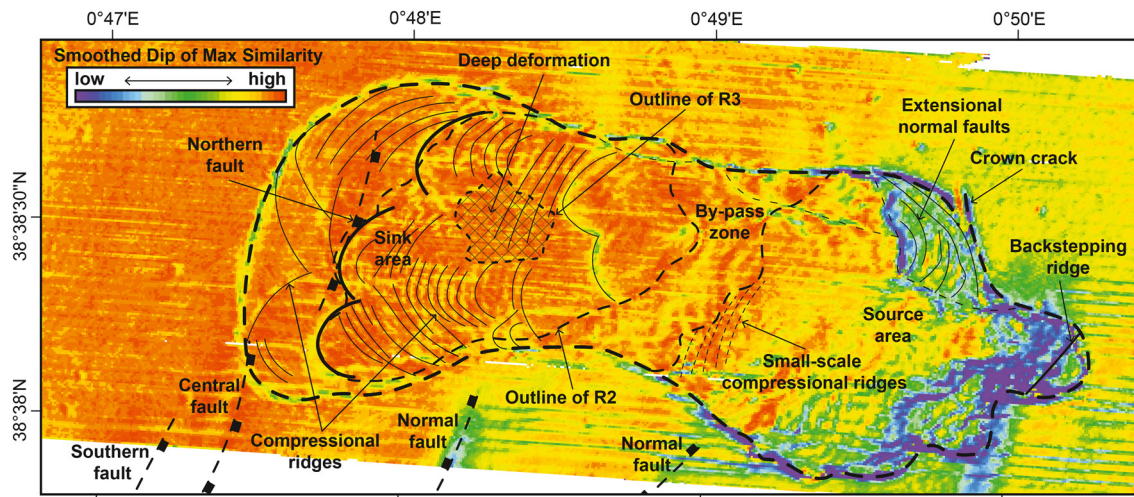


Figure 8. Seismic attribute map calculated on SFR (Smoothed Dip of Maximum Similarity—RockSolid Attributes from the 3D reflection seismic data). Kinematic features such as extensional ridges within the limited mobilized material within the northern source area, small-scale compressional ridges immediately upslope of the by-pass zone, and numerous compressional ridges throughout the sink area are highlighted. The backstepping ridge indicates easternmost headscarp retrogression during the secondary failure (Figure 10).

downslope of the present-day headscarp was mobilized a limited distance downslope during the secondary failure (Figure 9). Consequently, the crown-crack also developed during this stage as one of the latest features. Ultimately, the crown-crack is the expression of retrogression that was unable to propagate further upslope probably controlled by the gentler slope gradient within the northern source area.

6.3. Evolution and Emplacement of the Primary Failure

Unit 2 is thicker than Unit 1 (Figure 3) and the isochore map of both units shows a thinner central and southern source area (Figure 4c). This indicates the location from where most landslide material was evacuated as Unit 2 is thinned inside the scar of Ana Slide compared to outside of it, thus representing evacuation from the source area. Throughout the by-pass zone landslide material was neither added nor removed during the primary failure. The main accumulation features, that is, the three primary lobes, are located around 300–500 m upslope of the front of Ana Slide (Figures 2 and 8). Thus, landslide material mainly accumulated within the central sink area. This probably happened during the earliest part of the primary failure because landslide material did not reach all the way to the front of Ana Slide as documented by the location of thick material of Unit 2 immediately upslope of the northern fault (Figure 4c). During a later part of the primary failure, landslide material reached the northern sink area, constrained by the positive topographic relief along the northern lateral margin (Figures 2, 7c, and 7d) and orientation of the northern primary lobe further toward the west-north-west compared to the central primary lobe that is orientated more toward the west. The southern primary lobe formed at the latest part of the primary failure, as the central sink area was already infilled by previously accumulated landslide material. During the secondary failure landslide material ran out within the whole sink area, as shown by compressional ridges in the isochore map of Unit 1, which are located sub-parallel to and reach the front of Ana Slide (Figure 4a). If these compressional ridges were exclusively generated during the secondary failure or were also affected by the post-failure seafloor after the primary failure is unclear.

6.4. Evolution and Emplacement of the Secondary Failure

The difference in thickness of Unit 1 between inside and outside the scar of Ana Slide is less significant within the sink area compared to Unit 2 (Figure 4a). In addition, Unit 1 is generally thinner throughout the study area compared to Unit 2 (Figure 3). Hence, the secondary failure involved relatively small amounts of landslide material compared to the primary failure. Compressional ridges observed in Unit 1 are located sub-parallel to and reach the front of Ana Slide and characterize one overall orientation of movement of landslide material during the secondary failure (Figure 4a). During this, landslide material was fully mobilized throughout the by-pass zone

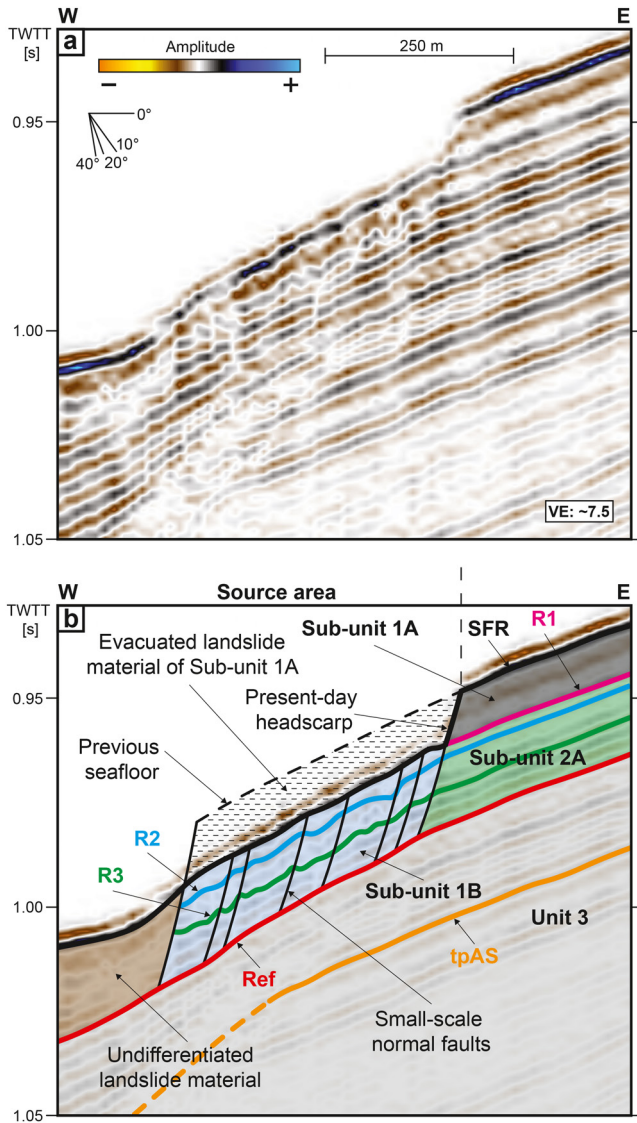


Figure 9. (a) Uninterpreted profile (re-processed 2D data) through the northern source area (see location in Figure 2). (b) Interpreted profile showing (re-processing 2D data) showing material formerly of Sub-unit 2A (light blue) previously *in-situ* and un-affected. This material changed apparent stratigraphic identity during the secondary failure with the general of small-scale extensional normal faults that terminate at depth above Ref. These small-scale extensional normal faults document that the material of Sub-unit 1B (formerly Sub-Unit 2A) was deformed *in-situ* by the evacuation of landslide material of Sub-unit 1A above. A visual comparison of the 3D and 2D reflection seismic profiles is presented in Figures S6–S11 of Supporting Information S1.

above R1 as the thickness of Sub-unit 1B in this area equals that of Sub-unit 1A outside the scar of Ana Slide. Thus, neither accumulation nor deposition of landslide material occurred in the by-pass zone during the secondary failure. In addition, the headscarp retrogressed the farthest eastwards, that is, some hundred meters upslope of the location of the steepest slope gradient within the easternmost headscarp (Figure 3). The shoulders and the eastern-most headscarp outline consequently smaller areas while the backstepping ridge marks the location of the latest retrogression (Figure 8). Compared to the primary failure with the extensive evacuation of landslide material from the source area, less extensive evacuation from the source area occurred during the secondary failure. Further, undifferentiated landslide material represents both ponded material from the primary and secondary failures.

Material located between Ref and SFR immediately downslope of the headscarp within the northern source area shows small-scale extensional ridges linked to small-scale normal faults (Figure 9). This material was initially linked to Sub-unit 2A, but it was not mobilized during the primary failure. This material occurs within the northern source area at present and thus also remained *in-situ* during the primary failure. After the primary failure hemipelagic sedimentation deposited Unit 1 between R1 and SFR. During the secondary failure material of Unit 1 was evacuated from the northern source area and the headscarp retrogressed to the location of the present-day headscarp (Figure 10c). Since inherent material of Unit 2 at this location shows small-scale extensional ridges but was not fully evacuated, we interpret this material to have experienced limited downslope mobilization during the secondary failure. In addition, this material changed apparent stratigraphic identity from being part of Unit 2 to material of Sub-unit 1B because it was affected first during the secondary failure.

6.5. Structural and Morphological Controls on Landslide Emplacement

The emplacement of Ana Slide encompasses the active processes of evacuation, mobilization, and accumulation of landslide material. A small amount of material represented by the “undifferentiated landslide material” ponded upslope against the by-pass zone. This material was unable to step up and above R1 and the by-pass zone that acted as an obstacle to the downslope propagation of landslide material. Also, undifferentiated landslide material partly remained at this position during the primary and secondary failures but if the small-scale thrust faults were generated mainly during primary or secondary failure is inconclusive (Figure 6). The largest part of the landslide material mobilized during both failures stepped up and over by-pass zone and accumulated within the sink area (Figures 3c and 4b).

Moernaut and De Batist (2011) propose that when a failure is able to overrun an obstacle and emerges frontally, the source area will evacuate in an unconfined manner. The failing landslide material will accelerate gaining kinetic energy and will be able to empty the source area of landslide material.

As the primary failure of Ana Slide involved larger amounts of material than the secondary failure this may be an explanation as to why the secondary failure left some material ponded against the by-pass zone. The small-scale compressional thrust faults within the undifferentiated landslide material might thus have been created during the primary failure, similar to compressional thrusts faults toward the front of submarine landslide as the movement experiences basal step-up. Alternatively, during the secondary failure deformational processes during the by-pass of landslide material occurred. Similar ponding also occurred at the northern fault, which acted as another obstacle against the downslope propagation of landslide material within the central sink area (Figure 4b). This fault

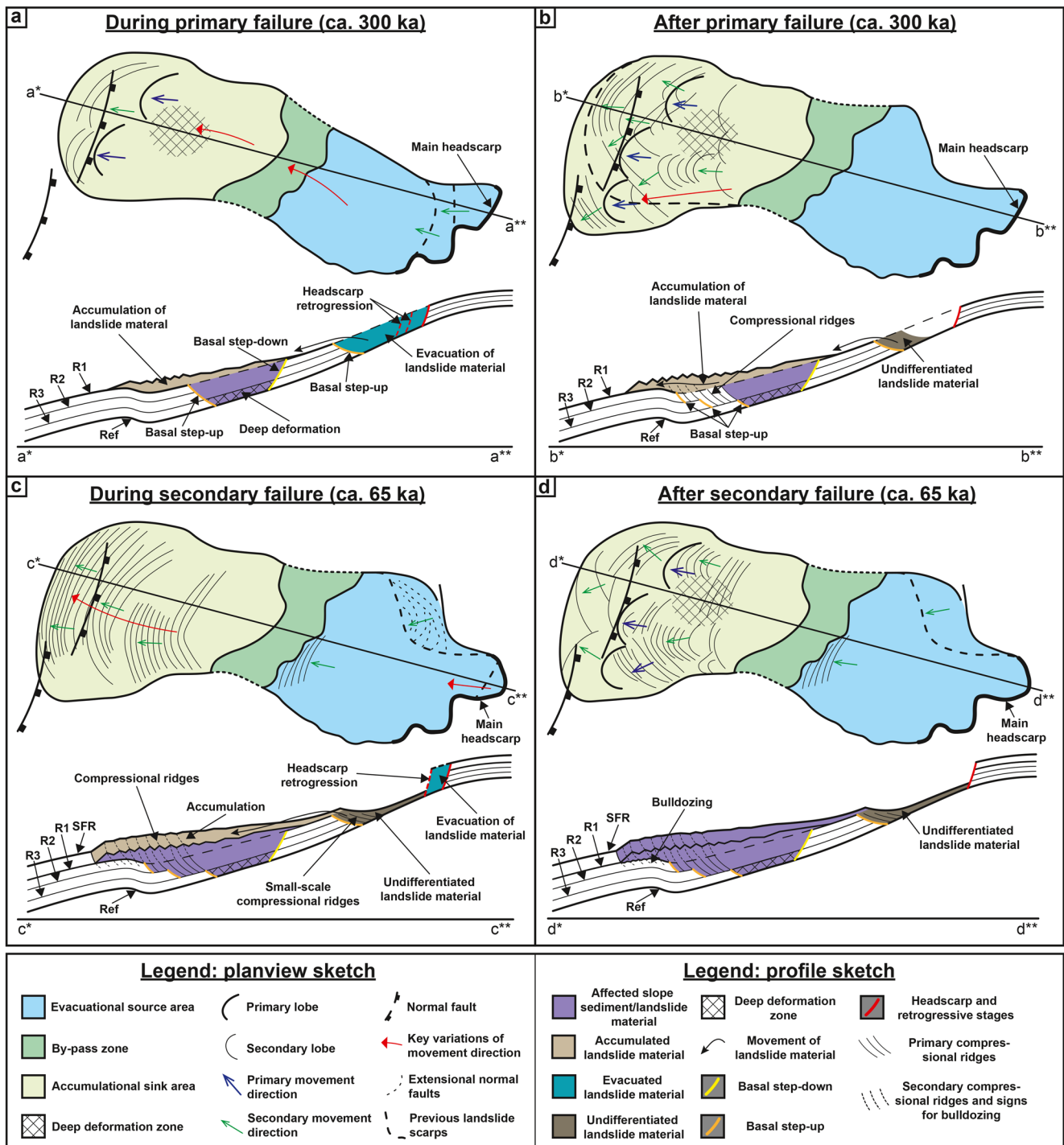


Figure 10. Interpretative development sketch of Ana Slide. (a) Early stage of primary failure (ca. 300 ka.). The central and northern primary lobes are formed within the sink area that are sourced by material evacuated from the central and southern source area. These primary lobes relate to retrogression of secondary headscarps inside the eastern source area. *In-situ* deformation is induced around 300–500 m upslope of the northern fault inside the sink area. (b) Consecutive headscarp retrogression during the late stage of the primary failure (at 300 ka.). This process presumably evacuated more landslide material from the source area and generated the southern primary lobe within the southern sink area with generation of compressional ridges throughout the sink area. (c) Limited mobilization of material within the northern source area (ca. 65 ka.). The easternmost headscarp is generated by retrogression upslope of the backstepping ridge. Landslide material ran out within the whole sink area and generated compressional ridges sub-parallel with the front of Ana Slide. Small-scale compressional ridges were generated upslope of the by-pass zone linked to a structural control. (d) Compilation of kinematic features observed from the bathymetry, and slope gradient and seismic attribute map (at 65 ka. (present-day)) (Figure 9).

generated a local basin upslope of its location, which was infilled by landslide material from the primary failure. The infill smoothed the seafloor morphology and therefore landslide material mobilized during the secondary failure could have more easily ran out within the sink area and have reached all the way toward the front of Ana Slide. The northern fault acted as a controlling mechanism to the emplacement of Ana Slide and as an obstacle to the downslope propagation of mobilized landslide material mainly during the primary failure. This means that the seafloor was already affected by the central and northern faults prior to the primary failure. Hence, accumulated landslide material mainly of the primary failure is located NE-SW above the northern fault.

Strongly imprinted on tpAS, there exists a compression fold at tpAS immediately toward the west of the by-pass zone (Figures 3 and 6). The small-scale compressional thrusts faults were likely created by the interplay of frontal emergence of both stages of failure from Ref toward R1 between the source and by-pass zone and from a morphological jump for the downslope propagation of failure controlled by the compression fold during the primary and secondary failure.

Although landslide material accumulated primarily around 300–500 m upslope of the front of Ana Slide and upslope of the northern fault (Figures 4b, 4c, and 8), compressional ridges are located at depth toward the front of Ana Slide (Figure 3c). This is observed between R3 and R2 and immediately below R1 (Figure 3). These compressional ridges were presumably generated by landslide material from the primary failure that bulldozed inherently un-affected slope sediment because the amount of landslide material was significantly larger during the primary than the secondary failure. Furthermore, the compressional ridges are located at depth below R1 that constituted the seafloor at the time of the primary failure and are thus the result of bulldozing landslide material into the footwall of the northern fault.

6.6. Causal Factors Between Fault Activity and Landsliding

The southern, central, and northern faults represent slope anti-thetic normal faults of unknown origin (Figures 3, 5c, and 5d). These faults modified the seafloor in the study area prior to the occurrence of Ana Slide. The faults could have acted as fluid conduits that resulted in gas-charging of the shallow sub-surface. Gas-charging may reduce the frictional resistance of sediments, thus acting as a pre-conditioning to slope failure (e.g., Kaminski et al., 2021). Seismogenic fault activity might have acted as a trigger mechanism. However, the role of the faults in both pre-conditioning and triggering remains inconclusive.

6.7. Identification of the Basal Shear Surfaces

Classic models for landslides describe one common basal shear surface through the source area, translational domain and sink area with possible upslope secondary basal shear surfaces created during retrogression (e.g., Bull et al., 2009; Frey-Martínez et al., 2005, 2006). This does not hold true for Ana Slide because two basal shear surfaces existed inside the sink area for the primary and the late-stage failures. Within the source area, the basal shear surface followed Ref toward the by-pass zone. Throughout the by-pass zone, the basal shear surface of the primary failure stepped up and over *in-situ* and un-affected material and thus followed the seafloor at the time of failure (Figures 3, 10a, and 10b). Within the sink area during the primary failure the basal shear surface was located at the seafloor (represented by R1 outside the scar of Ana Slide) while the base of deformation reached to depth of Ref (Figure 3). It is not easily discernible in the reflection seismic data, but the basal shear surface in the sink area during the primary failure must have been located within sub-units 2B and 2C (Figure 3c) as these units are significantly thicker than Sub-unit 2A (Figures 3c and 4b). During the secondary failure the basal shear surface inside the source area was located above Ref inside undifferentiated landslide material (Figures 3 and 10c). While we cannot conclusively constrain the identity of undifferentiated landslide material within the source area, landslide material of the secondary failure was certainly mobilized above Ref and stepped up and over *in-situ* and unaffected slope sediment of the by-pass zone. Inside the by-pass zone and into the sink area the basal shear surface at the time of the secondary failure was located between R1 and SFR (Figure 10c).

Both the primary and secondary failures of Ana Slide were frontally emergent inside the source area because they stepped up toward the seafloor (R1) immediately upslope of the by-pass zone at the time of their respective occurrences (Figures 10a and 10c). Inside the sink area landslide material ran up against un-affected slope sediment downslope and thus both the primary and secondary failures were frontally confined within the sink area.

6.8. *In-Situ* Deformation Beneath Landslide Deposit

In recent years, a new consensus arose from studies of Sobiesiak et al. (2016, 2018) distinguishing a set of basal interactions, that is, basal erosion, liquefaction and substrate deformation. These authors proposed that, in principle, basal interaction of some form might occur within the substrate beneath an overriding mass of landslide material. On the seismic scale (5–50 m) these deformational processes produce cryptic reflections that appear as low-amplitude transparent to chaotic seismic facies (e.g., Ford et al., 2021).

For Ana Slide, the basal shear surface of the primary failure is identified to have been located at the depth of R1 parallel to Ref inside sub-units 2B and 2C (stippled dark blue line in Figure 3c). Consequently, sub-units 2B and 2C involve material that respectively experienced apparent high and moderate degrees of deformation assuming that the increasingly chaotic seismic character corresponds to increasing *in-situ* deformation (Figure 3) while leaving the by-pass zone un-affected.

During the primary failure of Ana Slide landslide material mainly reached the central sink area upslope of the northern fault (Figure 4b). Accumulated landslide material was rapidly deposited within the sink area and able to load un-affected slope sediment. Sun and Alves (2020) show that MTDs generally have lower water content, porosity and permeability compared to background hemipelagic sediments. The rapid deposition of this relatively low water content, porosity, and permeability landslide material during the primary failure could have induced overpressure within hemipelagic sediments immediately beneath. This then acted as a “sealing lid” and loaded the seafloor and slope sediment of Unit 2A that change stratigraphic identify to Sub-Unit 2B and 2C. Low-amplitude seismic facies in Sub-unit 2B could be related to discontinuous reflectors due to some small-scale disturbance and interruptions of sediment layering because rapidly deposited landslide material prevented the vertical dissipation of excess pore pressure. The observation that the location of *in-situ* deformation is congruent with the location of thickest landslide deposits involved during the primary failure supports this hypothesis. A similar process has been suggested by Lenz et al. (2018) offshore Oregon, where rapidly deposited sedimentary blocks induced *in-situ* deformation within the immediate substrate. Deformation in Ana Slide possibly was further facilitated by the presence of fluids and gas as proposed by Berndt et al. (2012) in the overburden immediately above and east of the northern fault along Ref. The location of *in-situ* deformation within the sink area could thus be linked with deformation that only occurred some hundred meters upslope of the northern fault. The extent of *in-situ* deformation furthermore coincides with the fluid and gas migration vertically along the northern fault and horizontally along Ref approximately to the downslope extent of the by-pass zone (Figure 4).

Alternatively, the accumulating landslide material sheared the substrate below the interpreted basal shear surface down to Ref (Figure 3). Similar processes have been described for debris avalanches from a volcanic island in Papua New Guinea (Kühn et al., 2021). Since the by-pass zone has not been part of Ana Slide and remained un-affected during the primary and secondary failures shearing would also have deformed material within the by-pass zone beneath R1 and down to Ref. Hence, shearing of overriding landslide material seems improbable to explain the observed deformation.

It is, however, questionable if the process of loading is solely responsible for the observed deformation. Ultimately, we are unable to differentiate the loading from the shearing hypothesis, as they may have acted at the same time. Landslides develop dynamically over large distances, and several factors and processes may be responsible for kinematic features, with both processes acting concomitantly.

6.9. Implications for the Development and Emplacement of Submarine Landslides

Our detailed analysis of Ana Slide reveals emplacement processes differing from those previously suggested, most often based on bathymetry and 2D reflection seismic data. Lastras et al. (2004) interpreted the by-pass zone to be comprised of rotated intact blocks and the *in-situ* sediment deformation in the sink area as part of Ana Slide. Consequently, the estimated landslide volume was much larger compared to the model we propose, in which the deformed and affected slope sediment inside the sink area was not per se part of landslide material of Ana Slide. Furthermore, Ana Slide was interpreted as an exemplary frontally confined landslide. In contrast, we show that it is a mixed system. In the following, we use the example of Ana Slide (imaged in its entirety) to identify potential pitfalls when analyzing emplacement processes of submarine landslides that are only partly imaged.

6.9.1. Intact Blocks

Stratified and non-disturbed areas in reflection seismic profiles within submarine landslides are a common observation and are usually referred to as “intact blocks” (e.g., Bull et al., 2009). It is only with 3D reflection seismic data covering the whole landslide that we were able to identify that the by-pass zone (interpreted as an intact block previously) was not part of the landslide but remained entirely un-affected. Consequently, caution must be taken when areas with conformal stratigraphic layering are identified within the landslide as these may represent *in-situ* and un-affected slope sediment instead of mobilized blocks. Furthermore, the fact that previously identified blocks inside a MTD may represent *in-situ* slope sediment greatly depends on their location and kinematics within the MTD (e.g., Bull et al., 2009). Ultimately, the MTD term is kinematically problematic, as it infers that the material was moved and involved by the failure.

6.9.2. Deformation of Underlying Sediment

We suggest that the deposition of landslide material is able to deform a thick interval underneath. This highlights the potential of deformational processes observed for Ana Slide to penetrate deep into the subsurface (Figure 3). It is important to note that affected and deformed slope sediment within the sink area may not represent actual MTD material and should not be attributed to the actual volume of material mobilized during the landslide.

6.9.3. Complex Failure

The scar of Ana Slide includes a wide source area with additional upslope retrogressing headscarps, a narrow by-pass zone, and a wide lobe-shaped sink area (Figure 2). Such a geometry might indicate a relatively “simple” failure and emplacement process, in which the one age obtained through sampling represents the approximate timing of this landslide. However, our detailed analysis shows that Ana Slide involved multiple failure stages and complex emplacement processes, pointing to an overall complex behavior that likely is reproduced in other submarine landslides.

6.9.4. Landslide Volumes

The volume of Ana Slide inferred from the volume of material accumulated inside the sink area is around 0.058 km^3 ($\pm <10\%$) calculated between Ref and R1. This volume is significantly smaller than that calculated by Lastras et al. (2004) of 0.14 km^3 and does likely not represent the tsunamigenic material but much *in-situ* deformation that does not add to the tsunamigenic potential of Ana Slide. It is worth acknowledging that the slide volume is not the only important parameter controlling the tsunamigenic potential of a submarine landslide. It could be even with a smaller volume, if it undergoes higher acceleration, that it induces could induce a similar magnitude tsunami compared with larger lower acceleration landslides.

7. Conclusions

Our detailed examination of a high-resolution 3D seismic data set covering an entire submarine landslide (Ana Slide) reveals important new insights into the kinematic development of this landslide. Ana Slide is the result of two main stages of failure: a more voluminous primary failure and a smaller secondary failure separated by a time-lag of several hundreds of thousands of years. Both the primary and secondary failure were frontally emergent from the source areas and frontally confined in the sink area. A by-pass zone consisting of undisturbed *in-situ* slope sediment separates the source and the sink areas. Sediments underneath the deposit of Ana Slide show evidence for deformation, which was likely caused by rapid loading of the seafloor by the deposit. Both the by-pass zone and *in-situ* deformation had previously been accounted as landslide material. Consequently, these previous studies overestimated the volume and therewith the tsunamigenic potential of Ana Slide.

If similar processes of emplacement and *in-situ* deformation below a basal shear surface deep into the subsurface are at play for other submarine landslides remains speculative but such processes are not inconceivable for frontally emergent landslides.

Data Availability Statement

2D and 3D reflection seismic data used for integrated seismic interpretation of Ana Slide presented in this study are available at World Data Centre Pangaea (<https://doi.pangaea.de/10.1594/PANGAEA.943506> (3D reflection seismic data); <https://doi.pangaea.de/10.1594/PANGAEA.943523> (2D re-processed reflection seismic data)).

Acknowledgments

The 3D reflection seismic data was acquired as part of the EC-funded HERMIONE project (ref. 226354-HERMIONE). Also, the Spanish CONSOLIDER-INGENIO 2010 “GRACIE” project (ref. CSD2007-00067) contributed to this research. We thank the master and the crew of RRS Charles Darwin who facilitated data acquisition during voyage 178, and Frode Eriksen of VBPR, Oslo for technical support on the same cruise. IHS Markit provided academic licenses for KingdomSuite and Schlumberger for OMEGA. This study was supported by the DFG (Deutsche Forschungsgemeinschaft) Verbundprojekt UR 226/3-1 and GR 1024/35-1 by MU, Juergen Grabe of the TUHH, Hamburg, Germany, and CB. MC and GL acknowledge support from a Grups de Recerca Consolidats (excellence research groups) Grant to GRC Geociències Marines (ref. 2017 SGR 315) by the Government of Catalonia.

References

- Alves, T. M., & Cartwright, J. A. (2009). Volume balance of a submarine landslide in the Espírito Santo Basin, offshore Brazil: Quantifying seafloor erosion, sediment accumulation and depletion. *Earth and Planetary Science Letters*, 288(3–4), 572–580. <https://doi.org/10.1016/j.epsl.2009.10.020>
- Barrett, R., Lebas, E., Ramalho, R., Klauke, I., Kutterolf, S., Klügel, A., et al. (2020). Revisiting the tsunamigenic volcanic flank collapse of Fogo Island in the Cape Verdes, offshore West Africa. *Geological Society, London, Special Publications*, 500(1), 13–26. <https://doi.org/10.1144/SP500-2019-187>
- Berndt, C., Costa, S., Canals, M., Camerlenghi, A., De Mol, B., & Saunders, M. (2012). Repeated slope failure linked to fluid migration: The Ana submarine landslide complex, Eivissa Channel, Western Mediterranean Sea. *Earth and Planetary Science Letters*, 319(320), 65–74. <https://doi.org/10.1016/j.epsl.2011.11.045>
- Bondevik, S., Løvholt, F., Harbitz, C., Mangerud, J., Dawson, A., & Inge Svendsen, J. (2005). The Storegga Slide tsunami—Comparing field observations with numerical simulations. *Marine and Petroleum Geology*, 22(1–2), 195–208. <https://doi.org/10.1016/j.marpetgeo.2004.10.003>
- Bryn, P., Berg, K., Forsberg, C. F., Solheim, A., & Kvalstad, T. J. (2005). Explaining the Storegga Slide. *Marine and Petroleum Geology*, 22(1–2), 11–19. <https://doi.org/10.1016/j.marpetgeo.2004.12.003>
- Bugge, T., Befring, S., Belderson, R. H., Eidvin, T., Jansen, E., Kenyon, N. H., et al. (1987). A giant three-stage submarine slide off Norway. *Geo-Marine Letters*, 7(4), 191–198. <https://doi.org/10.1007/BF02242771>
- Bull, S., Cartwright, J., & Huuse, M. (2009). A review of kinematic indicators from mass-transport complexes using 3D seismic data. *Marine and Petroleum Geology*, 26(7), 1132–1151. <https://doi.org/10.1016/j.marpetgeo.2008.09.011>
- Canals, M., & Ballesteros, E. (1997). Production of carbonate particles by phyto-benthic communities on the Mallorca-Menorca shelf, north-western Mediterranean Sea. *Deep-Sea Research Part II Topical Studies in Oceanography*, 44(3–4), 611–629. [https://doi.org/10.1016/S0967-0645\(96\)00095-1](https://doi.org/10.1016/S0967-0645(96)00095-1)
- Cattaneo, A., Daniel, M., Alessandra, A., Miquel, C., Ben, D. M., Sara, L., et al. (2011). Age constraints and sediment properties of Ana Slide (Balearic Sea, Western Mediterranean) and implications on age dating of submarine landslides. *Geophysical Research Abstracts*, 13(1), 2011–6047.
- Clare, M., Chaytor, J., Dabson, O., Gamboa, D., Georgiopolou, A., Eady, H., et al. (2019). A consistent global approach for the morphometric characterization of subaqueous landslides. *Geological Society, London, Special Publications*, 477(1), 455–477. <https://doi.org/10.1144/SP477.15>
- del Valle, L., Gómez-Pujol, L., Fornós, J. J., Timar-Gabor, A., Anechitei-Deacu, V., & Pomar, F. (2016). Middle to Late Pleistocene dunefields in rocky coast settings at Cala Xuclar (Eivissa, Western Mediterranean): Recognition, architecture and luminescence chronology. *Quaternary International*, 407, 4–13. <https://doi.org/10.1016/j.quaint.2016.01.050>
- Farrell, S. G. (1984). A dislocation model applied to slump structures, Ainsa Basin, South Central Pyrenees. *Journal of Structural Geology*, 6(6), 727–736. [https://doi.org/10.1016/0191-8141\(84\)90012-9](https://doi.org/10.1016/0191-8141(84)90012-9)
- Ford, J., Urgeles, R., Camerlenghi, A., & Gràcia, E. (2021). Seismic diffraction imaging to characterize mass-transport complexes: Examples from the Gulf of Cadiz, south west Iberian Margin. *Journal of Geophysical Research: Solid Earth*, 126(3). <https://doi.org/10.1029/2020JB021474>
- Frey-Martinez, J. F., Cartwright, J., & Hall, B. (2005). 3D seismic interpretation of slump complexes: Examples from the continental margin of Israel. *Basin Research*, 17(1), 83–108. <https://doi.org/10.1111/j.1365-2117.2005.00255.x>
- Frey-Martínez, J., Cartwright, J., & James, D. (2006). Frontally confined versus frontally emergent submarine landslides: A 3D seismic characterisation. *Marine and Petroleum Geology*, 23(5), 585–604. <https://doi.org/10.1016/j.marpetgeo.2006.04.002>
- Fruergaard, M., Piasecki, S., Johannessen, P. N., Noe-Nygaard, N., Andersen, T. J., Pejrup, M., & Nielsen, L. H. (2015). Tsunami propagation over a wide, shallow continental shelf caused by the Storegga Slide, southeastern North Sea, Denmark. *Geology*, 43(12), 1047–1050. <https://doi.org/10.1130/G37151.1>
- Hafliadason, H., Lien, R., Sejrup, H. P., Forsberg, C. F., & Bryn, P. (2005). The dating and morphometry of the Storegga Slide. *Marine and Petroleum Geology*, 22(1–2), 123–136. <https://doi.org/10.1016/j.marpetgeo.2004.10.008>
- Hafliadason, H., Sejrup, H. P., Nygård, A., Mienert, J., Bryn, P., Lien, R., et al. (2004). The Storegga Slide: Architecture, geometry and slide development. *Marine Geology*, 213(1–4), 201–234. <https://doi.org/10.1016/j.marpetgeo.2004.10.007>
- Harbitz, C. B., Løvholt, F., & Bungum, H. (2014). Submarine landslide tsunamis: How extreme and how likely? *Natural Hazards*, 72(3), 1341–1374. <https://doi.org/10.1007/s11069-013-0681-3>
- Haugen, K. B., Løvholt, F., & Harbitz, C. B. (2005). Fundamental mechanisms for tsunami generation by submarine mass flows in idealised geometries. *Marine and Petroleum Geology*, 22(1–2), 209–217. <https://doi.org/10.1016/j.marpetgeo.2004.10.016>
- Hodge, E. J., Richards, D. A., Smart, P. L., Ginés, A., & Matthey, D. P. (2008). Sub-millennial climate shifts in the western Mediterranean during the last glacial period recorded in a speleothem from Mallorca, Spain. *Journal of Quaternary Science*, 23(8), 713–718. <https://doi.org/10.1002/jqs.1198>
- Hühnerbach, V., & Masson, D. (2004). Landslides in the North Atlantic and its adjacent seas: An analysis of their morphology, setting and behaviour. *Marine Geology*, 213(1–4), 343–362. <https://doi.org/10.1016/j.marpetgeo.2004.10.013>
- Jackson, C. A.-L. (2011). Three-dimensional seismic analysis of megaclast deformation within a mass transport deposit; implications for debris flow kinematics. *Geology*, 39(3), 203–206. <https://doi.org/10.1130/G31767.1>
- Kaminski, P., Sager, T., Grabe, J., & Urlaub, M. (2021). A new methodology to assess the potential of conjectural trigger mechanisms of submarine landslides exemplified by marine gas occurrence on the Balearic Promontory. *Engineering Geology*, 295, 106446. <https://doi.org/10.1016/j.enggeo.2021.106446>
- Krastel, S., Li, W., Urlaub, M., Georgiopolou, A., Wynn, R. B., Schwenk, T., et al. (2019). Mass wasting along the NW African continental margin. *Geological Society, London, Special Publications*, 477(1), 151–167. <https://doi.org/10.1144/SP477.36>
- Kühn, M., Karstens, J., Berndt, C., & Watt, S. F. L. (2021). Seismic reconstruction of seafloor sediment deformation during volcanic debris avalanche emplacement offshore Sakar, Papua New Guinea. *Marine Geology*, 439, 106563. <https://doi.org/10.1016/j.marpetgeo.2021.106563>

- Kvalstad, T. J., Andresen, L., Forsberg, C. F., Berg, K., Bryn, P., & Wangen, M. (2005). The Storegga Slide: Evaluation of triggering sources and slide mechanics. *Marine and Petroleum Geology*, 22(1–2), 245–256. <https://doi.org/10.1016/j.marpetgeo.2004.10.019>
- Lackey, J., Moore, G., & Strasser, M. (2018). Three-dimensional mapping and kinematic characterization of mass transport deposits along the outer Kumano Basin and Nankai accretionary wedge, southwest Japan. *Progress in Earth and Planetary Science*, 5(1), 65. <https://doi.org/10.1186/s40645-018-0223-4>
- Lafuerza, S., Sultan, N., Canals, M., Lastras, G., Cattaneo, A., Frigola, J., et al. (2012). Failure mechanisms of Ana Slide from geotechnical evidence, Eivissa Channel, Western Mediterranean Sea. *Marine Geology*, 307–310, 1–21. <https://doi.org/10.1016/j.margeo.2012.02.010>
- Lastras, G., Canals, M., Amblas, D., Ivanov, M., Dennielou, B., Droz, L., & Akhmetzhanov, A. (2006). Eivissa slides, Western Mediterranean Sea: Morphology and processes. *Geo-Marine Letters*, 26(4), 225–233. <https://doi.org/10.1007/s00367-006-0032-4>
- Lastras, G., Canals, M., Urgeles, R., Hughes-Clarke, J. E., & Acosta, J. (2004). Shallow slides and pockmark swarms in the Eivissa Channel, Western Mediterranean Sea. *Sedimentology*, 51(4), 837–850. <https://doi.org/10.1111/j.1365-3091.2004.00654.x>
- Lenz, B., Sawyer, D., Phrampus, B., Davenport, K., & Long, A. (2018). Seismic imaging of seafloor deformation induced by impact from large submarine landslide blocks, offshore Oregon. *Geosciences*, 9(1), 10. <https://doi.org/10.3390/geosciences9010010>
- Løvholt, F., Bondevik, S., Laberg, J. S., Kim, J., & Boylan, N. (2017). Some giant submarine landslides do not produce large tsunamis: Giant landslide tsunamis. *Geophysical Research Letters*, 44(16), 8463–8472. <https://doi.org/10.1002/2017GL074062>
- Maillard, A., & Mauffret, A. (2013). Structure and present-day compression in the offshore area between Alicante and Ibiza island (Eastern Iberian Margin). *Tectonophysics*, 591, 116–130. <https://doi.org/10.1016/j.tecto.2011.07.007>
- Masson, D. G., Harbitz, C. B., Wynn, R. B., Pedersen, G., & Løvholt, F. (2006). Submarine landslides: Processes, triggers and hazard prediction. *Philosophical Transactions of the Royal Society A: Mathematical, Physical & Engineering Sciences*, 364(1845), 2009–2039. <https://doi.org/10.1098/rsta.2006.1810>
- Mauffret, A., Pascal, G., Maillard, A., & Gorini, C. (1995). Tectonics and deep structure of the north-western Mediterranean Basin. *Marine and Petroleum Geology*, 12(6), 645–666. [https://doi.org/10.1016/0264-8172\(95\)98090-R](https://doi.org/10.1016/0264-8172(95)98090-R)
- Micallef, A., Berndt, C., Masson, D. G., & Stow, D. A. V. (2008). Scale invariant characteristics of the Storegga Slide and implications for large-scale submarine mass movements. *Marine Geology*, 247(1–2), 46–60. <https://doi.org/10.1016/j.margeo.2007.08.003>
- Mitchum, R. M., Jr., Vail, P. R., & Thompson, III, S. (1977). Seismic stratigraphy and global changes of sea-level, Part 2: The depositional sequence as a basic unit for stratigraphic analysis. In C. E. Payton (Ed.), *Seismic stratigraphy—Applications to hydrocarbon exploration* (Vol. 26, pp. 53–62). American Association of Petroleum Geologists Memoir.
- Moernaut, J., & De Batist, M. (2011). Frontal emplacement and mobility of sublacustrine landslides: Results from morphometric and seisstratigraphic analysis. *Marine Geology*, 285(1–4), 29–45. <https://doi.org/10.1016/j.margeo.2011.05.001>
- Nugraha, H. D., Jackson, C. A.-L., Johnson, H. D., & Hodgson, D. M. (2020). Lateral variability in strain along the toewall of a mass transport deposit: A case study from the Makassar Strait, offshore Indonesia. *Journal of the Geological Society*, 177(6), 1261–1279. <https://doi.org/10.1144/jgs2020-071>
- Ogata, K., Mountjoy, J. J., Pini, G. A., Festa, A., & Tinterri, R. (2014). Shear zone liquefaction in mass transport deposit emplacement: A multi-scale integration of seismic reflection and outcrop data. *Marine Geology*, 356, 50–64. <https://doi.org/10.1016/j.margeo.2014.05.001>
- Panieri, G., Camerlenghi, A., Cacho, I., Cervera, C. S., Canals, M., Lafuerza, S., & Herrera, G. (2012). Tracing seafloor methane emissions with benthic foraminifera: Results from the Ana submarine landslide (Eivissa Channel, Western Mediterranean Sea). *Marine Geology*, 291–294, 97–112. <https://doi.org/10.1016/j.margeo.2011.11.005>
- Prior, D. B., Bornhold, B. D., & Johns, M. W. (1984). Depositional characteristics of a submarine debris flow. *The Journal of Geology*, 92(6), 707–727. <https://doi.org/10.1086/628907>
- Ryan, W. B. F., Carbotte, S. M., Coplan, J. O., O'Hara, S., Melkonian, A., Arko, R., et al. (2009). Global multi-resolution topography synthesis: Global multi-resolution topography synthesis. *Geochemistry, Geophysics, Geosystems*, 10(3), Q03014. <https://doi.org/10.1029/2008GC002332>
- Sawyer, D. E., Flemings, P. B., Dugan, B., & Germaine, J. T. (2009). Retrogressive failures recorded in mass transport deposits in the Ursa Basin, Northern Gulf of Mexico. *Journal of Geophysical Research*, 114(B10), B10102. <https://doi.org/10.1029/2008JB006159>
- Sobiesiak, M. S., Kneller, B., Alsop, G. I., & Milana, J. P. (2016). Internal deformation and kinematic indicators within a tripartite mass transport deposit, NW Argentina. *Sedimentary Geology*, 344, 364–381. <https://doi.org/10.1016/j.sedgeo.2016.04.006>
- Sobiesiak, M. S., Kneller, B., Alsop, G. I., & Milana, J. P. (2018). Styles of basal interaction beneath mass transport deposits. *Marine and Petroleum Geology*, 98, 629–639. <https://doi.org/10.1016/j.marpetgeo.2018.08.028>
- Steventon, M. J., Jackson, C. A.-L., Hodgson, D. M., & Johnson, H. D. (2019). Strain analysis of a seismically imaged mass-transport complex, offshore Uruguay. *Basin Research*, 31(3), 600–620. <https://doi.org/10.1111/bre.12337>
- Sun, Q., & Alves, T. (2020). Petrophysics of fine-grained mass-transport deposits: A critical review. *Journal of Asian Earth Sciences*, 192, 104291. <https://doi.org/10.1016/j.jseae.2020.104291>
- Tuccimei, P., Fornós, J. J., Ginés, A., Ginés, J., Gràcia, F., & Mucedda, M. (2007). Sea level change at Capo Caccia (NW Sardinia) and Mallorca (Balearic Islands) during oxygen isotope substage 5e, based on Th/U datings of phreatic overgrowths on speleothems. *Geomorfologia Litoral i Quaternari. Homenatge a Joan Cuerda Barcelo. Monografies de La Societat d'Historia Natural de Les Balears*, 14, 121e136.
- Varnes, D. (1978). Slope movement types and processes. *Transportation Research Board Special Report* (p. 176).
- Voight, B., Janda, R., Glicken, H., & Douglass, P. (1983). Nature and mechanics of the Mount St. Helens rockslide-avalanche of 18 May 1980. *Géotechnique*, 33(3), 243–273. <https://doi.org/10.1680/geot.1983.33.3.243>
- Völker, D. J. (2010). A simple and efficient GIS tool for volume calculations of submarine landslides. *Geo-Marine Letters*, 30(5), 541–547. <https://doi.org/10.1007/s00367-009-0176-0>